Journal of Alloys and Compounds 1018 (2025) 179151

Contents lists available at ScienceDirect

Journal of Alloys and Compounds

journal homepage: www.elsevier.com/locate/jalcom

Review

Current progress in strengthening, plastic deformation and thermal stability of Mg alloys

Zhenghao Li [a], Mengning Xu [a], Yang Cao [a,b,*], Yonghao Zhao [a,b,*]

[a] Nano and Heterogeneous Materials Center, Nanjing University of Science and Technology, Nanjing 210094, China
[b] School of Materials Science and Engineering, Hohai University, Changzhou 213200, China

ARTICLE INFO

Keywords:
Mg alloys
Strengthening mechanisms
Deformation mechanisms
Thermal stability

ABSTRACT

Magnesium (Mg) alloys are considered a class of "green engineering materials" with the huge potential for industrial applications. However, Mg alloys still have some yet-to-be-solved deficiencies, such as low yield strength, low fracture toughness, poor ductility and low corrosion resistance, in comparison to lightweight aluminum and titanium alloys, and thus severely limiting large-scale applications of Mg alloys. This review covers recent progresses on the processing techniques, materials strengthening methods, deformation mechanisms and thermal stability of Mg and Mg alloys. Future perspectives on physical characteristics of Mg alloys, development of multi-functional Mg alloys and development of advanced Mg alloy processing techniques are provided.

1. Introduction

Magnesium (Mg) alloys are a class of light-weight materials, as if created to address the energy crisis that is currently being battled by mankind. Mg are abundant in earth crust and recyclable from end products [1]. Mg has a low density that is only two-thirds of aluminum (Al) and one-quarter of iron. Mg alloys offer excellent electromagnetic shielding and damping capacity, are ideal for packaging and shielding electronic products [2]; They are biodegradable and non-toxic to the human body, and are thus safe for orthopedic implant [3,4]. These abovementioned properties made Mg alloys very attractive to researchers and engineers from various communities and industries [5]. For all potential applications of Mg and its alloys, the mechanical properties are always concerned [6–8]. However, the absolute strength of Mg alloys is the lowest among the major structural materials, can hardly meet the demands of load-bearing structural components. On the other hand, due to the inherent hexagonal close-packed (HCP) crystal structure and insufficient number of easy slip systems, Mg alloys are difficult to sustain homogeneous plastic deformation, and thus in most cases showing poor ductility and formability [9]. Nevertheless, similar to many other metallic materials, Mg alloys also face the trade-off between strength and ductility, therefore it is very difficult to improve the strength of Mg alloys via conventional cold working methods.

With hope and virtue, whatever the difficulties, materials scientists grasp the nettle of strength-ductility dilemma and develop Mg alloys with improved mechanical properties. To date, the feasible methods for improving mechanical properties of Mg alloys are still alloying and plastic deformation. For alloying Mg based metals, Al, Zn, and Ca are popular choice of solutes, moreover, rare earth (RE) elements are found especially advantageous if cost is not the major concern. By adjusting the compositions, solid solution, precipitation and/or complexion strengthening effects can be realized to enhance the strength, and meanwhile non-basal slip can be promoted to reduce plastic anisotropy and thus to improve the ductility [10–12]. Plastic deformation can generate many sorts of defects including grain boundaries (GBs), twin boundaries, dislocations and stacking faults (SFs) to increase the resistance against dislocation slip and thus to increase the strength of the Mg alloys [13–15]. For Mg alloys, grain refinement not only enhances the strength, but also improves the ductility by reducing the propensity of deformation twinning and increasing the propensity of non-basal slip [8,16]. To date, severe plastic deformation (SPD) techniques are well developed to achieve significant strengthening results for Mg alloys. However, the mechanical configurations of SPD methods, which are designed particularly for imposing high strains, on the other hand strictly limit the size and shape of the workpiece [17]. In recent years, the rotary swaging (RS) process which is capable of imposing high-frequency pulse loading and high strain rates, has shown promising results for processing Mg alloys [18–20]. During RS, the radially placed

* Corresponding authors at: Nano and Heterogeneous Materials Center, Nanjing University of Science and Technology, Nanjing 210094, China.
E-mail addresses: y.cao@hhu.edu.cn (Y. Cao), yhzhao@njust.edu.cn (Y. Zhao).

https://doi.org/10.1016/j.jallcom.2025.179151
Received 6 January 2025; Received in revised form 8 February 2025; Accepted 10 February 2025
Available online 12 February 2025

dies strike on a tube or rod workpiece to impose compressive stress and strain in the radial directions, and meanwhile the workpiece is free to elongate in the axial direction. The mechanical configuration of RS machine allows the workpiece with theoretically unlimited length to be processed, and is ready for upgrade and expansion of modules including automatic workpiece feeding and continuous heat-treatment.

There have been quite a few review papers focusing on specific conventional deformation and SPD processing methods, and the related strengthening mechanisms for Mg alloys [21–26]. However, due to the recently fast development of Mg alloys and the associated processing methods, the published review papers may seem out-of-date for some aspects, e.g., the development of Mg alloys with improved thermal stabilities and RS processing Mg alloys have not been systematically reviewed. In this paper, in Section 2, we first revisit the fundamental characteristics and properties of Mg alloys and then classify the popular grades of Mg alloys. In Section 3, comprehensive review is done on the popular techniques used for strengthening Mg alloys, with a particular focus on the RS method; The fundamental strengthening mechanisms induced by the processing techniques are accordingly reviewed. In Section 4, we firstly revisited the deformation mechanisms in Mg alloys; Then we reviewed the methods that have been developed for enhancing ductility of Mg alloys with respect to the deformation mechanisms. In Section 5, we discussed the thermal stability of Mg alloys, and systematically reviewed the importance and fundamental concepts of introducing solute segregation, linear complexion, precipitation and reinforcement particles for improving the thermal stability. Section 6 provides the future perspectives in regarding the developments of advanced Mg alloys and the corresponding industrial processing techniques.

2. Fundamental aspects of Mg alloys

2.1. Characteristics of Mg alloys

The first research craze on Mg alloys occurred before World War II, although steels and Al alloys were by then still favored in both industries and research due to low cost and mature processing technologies. However, when the global energy crisis and global warming raised awareness across the world in 21st century, lightweight metallic materials, especially Mg alloys have again become the hot research and development topic [24,27,28]. Engineers and scientists have always had a special fondness for Mg alloys for the unique properties summarized in Fig. 1.

Mechanical properties: Mg alloys belong to the group of the lightest structural materials. They have high specific strength, ranking second only to titanium (Ti) alloys, and the highest specific stiffness among all known metallic materials. For the purposes of weight reduction and energy conservation, engineers and scientists are keen to explore the potential applications of Mg alloys in transportation, aerospace, and national defense industries etc. [29–31].

Physical properties: Mg alloys have excellent damping capacity and noise reduction functionalities, electrical conductivity, thermal conductivity and electromagnetic shielding properties, and have become the preferred structural material for the 3 C (computers, communication devices, and consumer electronics) electronics industry.

Environmental resources: The Earth has abundant reserves of Mg. Mg is among the top ten most abundant elements in nature, accounting for ~2 % of the Earth's crust by mass and ~0.13 % of seawater by mass [1]. While, China's Mg reserve ranks the first in the world. Mg is recyclable, biodegradable, environmentally friendly and non-toxic to the human body [32].

In view of the abovementioned advantages, Mg alloys are considered the most promising "green engineering materials" in the 21st century. However, Mg alloys also have some deficiencies, such as low strength, low fracture toughness [10,33], poor plastic deformation ability [34,35] and poor corrosion resistance [36,37], in comparison to lightweight Al and Ti alloys, and thus large-scale industrial applications of Mg alloys are yet to be feasible. Scientists have devoted tremendous efforts to eliminate deficiencies in Mg alloys via alloying and microstructural architecture. In recent years, the top international journals "Nature" and "Science" have continuously reported breakthroughs in the field of Mg alloys [34,35,38–40].

2.2. Types of Mg alloys

Based on the processing method, Mg alloys can be categorized into deformation Mg alloys and cast Mg alloys. In general, the performance of deformation Mg alloys is better than that of cast Mg alloys. Based on the composition, Mg alloys can be categorized into Mg-Li, Mg-Al, Mg-Zn and Mg-Mn based alloys, and Mg-RE series alloys, as shown in Fig. 2.

Mg-Li based alloys: They have the lowest density (1.35–1.65 g/cm^3) among metallic structural materials, and very good formability. The crystal structure of Mg-Li alloys can change with respect to the content of Li element. When the Li content is less than 5 wt%, the alloy is an HCP α-Mg solid solution; when the Li content is between 5 wt% - 11 wt%, the alloy has the two-phase structure consisting of HCP α-Mg solid solution phase and body-centered cubic (BCC) Li-rich β phase; when the Li content exceeds 11 wt%, the alloy becomes a BCC β-phase solid solution [41,42]. However, compared with many other Mg alloys, Mg-Li alloys have relatively low strength, poor corrosion resistance, which limit their

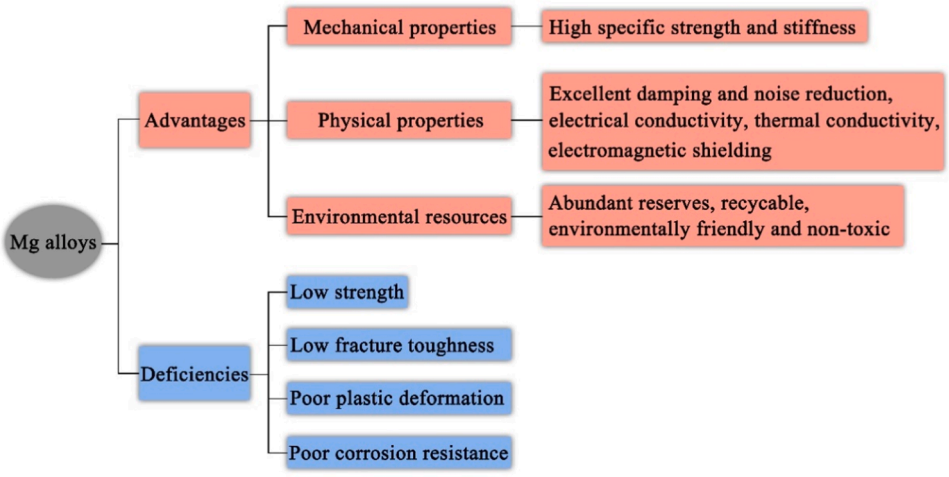

Fig. 1. Properties and deficiencies of Mg alloys.

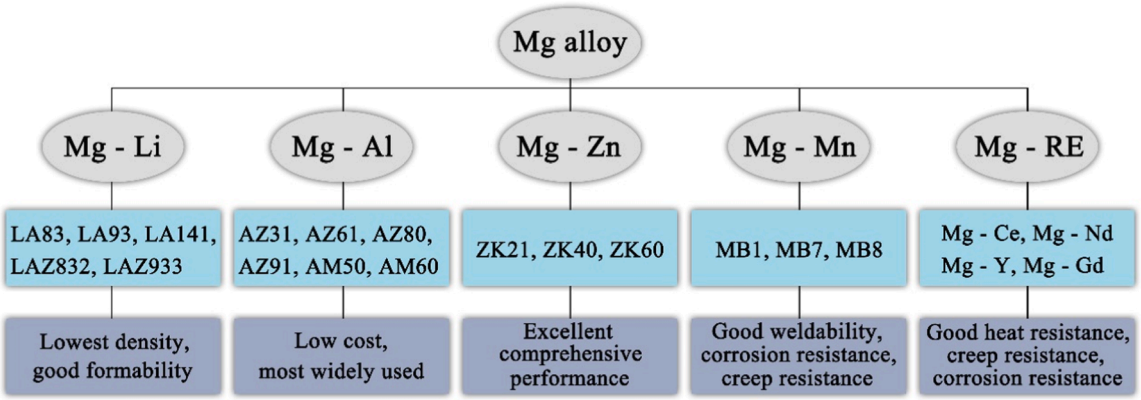

Fig. 2. Types of Mg alloys.

industrial applications. At present, the Mg-Li based alloys with the practical value in industry are LA83, LA93, LA141, LAZ832 and LAZ933 grades.

Mg-Al based alloys: The maximum solid solubility of Al in Mg is 11.5 % at 437°C and decreases with the decreasing temperature. The addition of Al can provide solid solution strengthening, precipitation strengthening and improved corrosion resistance to the Mg alloys. At present, Mg-Al based alloys are the most widely used Mg alloys, mainly because of the low cost. Recently, a large number of Mg-Al based alloys have been developed and put in use, such as Mg-Al-Zn, Mg-Al-Mn, Mg-Al-Si alloys. The commonly used grades are AZ31, AZ61, AZ80, AZ91, AM50, and AM60.

Mg-Zn based alloys: The maximum solid solubility of Zn in Mg is 3 % at 341°C, and it decreases significantly with decreasing temperature. The addition of Zn can also cause solid solution strengthening and precipitation strengthening. In practice, adding an appropriate amount of Zr to Mg-Zn alloy can refine the grain size and improve the mechanical properties. These Mg-Zn series alloys have high strength, good plasticity and corrosion resistance, and thus can provide excellent structural performance. The commonly used grades are ZK21, ZK40, and ZK60.

Mg-Mn based alloys: The maximum solid solubility of Mn in Mg is only 0.996 % at 653°C. Mn does not form any compound with Mg. The addition of Mn shows noticeable strengthening effect. In most cases, the main purpose of adding Mn is to refine the grain size and improve the weldability, corrosion resistance and creep resistance of the Mg alloy. The commonly used grades are MB1, MB7, and MB8.

Mg-RE series: RE elements have the unique extra nuclear orbital electron configuration, which may pose some interesting effects on the microstructure and properties of Mg alloys. The solid solubility of most RE elements in Mg is high, e.g., the maximum solid solubilities of Gd, Y, Er and Lu are 4.53 % at 548°C, 3.4 % at 467.4°C, 6.9 % at 570°C and 8.8 % at 616°C, respectively. Therefore, the addition of RE elements has the effects of solid solution strengthening and precipitation strengthening. Moreover, adding RE elements can also improve casting performance, corrosion resistance and thermal stability of the Mg alloys. The commonly used sub-series are Mg-Ce series, Mg-Nd series, Mg-Y series and Mg-Gd series.

3. Preparation of high strength Mg alloys and the strengthening mechanisms

To date, the high strength of Mg alloys is mainly achieved via two strengthening methods: (1) SPD for significant grain refinement [43], and (2) adding alloying elements for solid solution and precipitation strengthening [44–46].

3.1. Grain refinement via SPD

Usually, the strength of the metallic materials is enhanced by work hardening during plastic deformation. During SPD processes, drastic increase in dislocation densities leading to massive dislocation interactions and accumulations and thus rising up the flow stress to very high levels. The dislocation strengthening effect can be calculated by the Bailey-Hirsch formula [47,48]:

$$\sigma_{dis} = M\alpha Gb\rho^{\frac{1}{2}} \quad (1)$$

Where M is Taylor factor (mean orientation factor), which is typically the reciprocal of Schmid factor, α is a temperature dependent constant, G is the shear modulus, b is the magnitude of Burgers vector, ρ is the density of dislocations.

Massive dislocation interactions and accumulations under the effect of increasing shear strain, can eventually lead to grain refinement. Grain refinement creates new GBs and reduces the mean free path for dislocation slip. A GB divides two neighboring grains with the same crystal structure but different orientations. GBs can be classified into high angle GB (HAGB, $\geq 15°$) and low angle GB (LAGB, $<15°$), based on the angle of orientation. Once a gliding dislocation encounters a GB, it will experience a dramatic change in stress state due to back-stress, image stress and coherency stress, resulting in stagnation or absorption of the incoming dislocation by the GB. By either way, more and more dislocations will accumulate on the GB and thus rising up the flow stress, leading to the GB strengthening effect. Therefore, the higher number of GBs in a unit volume the higher flow stress of the material; The GB strengthening effect is governed by the empirical Hall-Petch relationship [49]:

$$\Delta\sigma_{HP} = \sigma_0 + Kd^{-1/2} \quad (2)$$

Where σ_0 represents the intrinsic lattice friction stress, K is the Hall-Petch slope (Hall-Petch constant) and d is the average grain size.

Different from the conventional metal forming processes, such as extrusion, rolling and forging, the SPD processes can impose very large strains and/or high strain rates, which in turn cause significant grain refinement to the ultrafine (100 nm $< d \leq$ 1 μm) and even nanocrystalline ($d \leq$ 100 nm) regimes without premature failure. The commonly used SPD methods are accumulative roll bonding (ARB), cyclic extrusion-compression (CEC), equal-channel angular pressing (ECAP), multi-directional forging (MDF), high-pressure torsion (HPT), friction stir processing (FSP), surface mechanical attrition treatment (SMAT) and surface mechanical grinding treatment (SMGT) [17,50]. Fig. 3 shows schematics of some SPD processes.

Table 1 collects the grain sizes, mechanical properties, sample sizes of high-strength Mg alloys processed by SPD methods in the last decade [49,51–110]. The Mg-8Gd-3Y-0.4Zr alloy processed by RS shows the

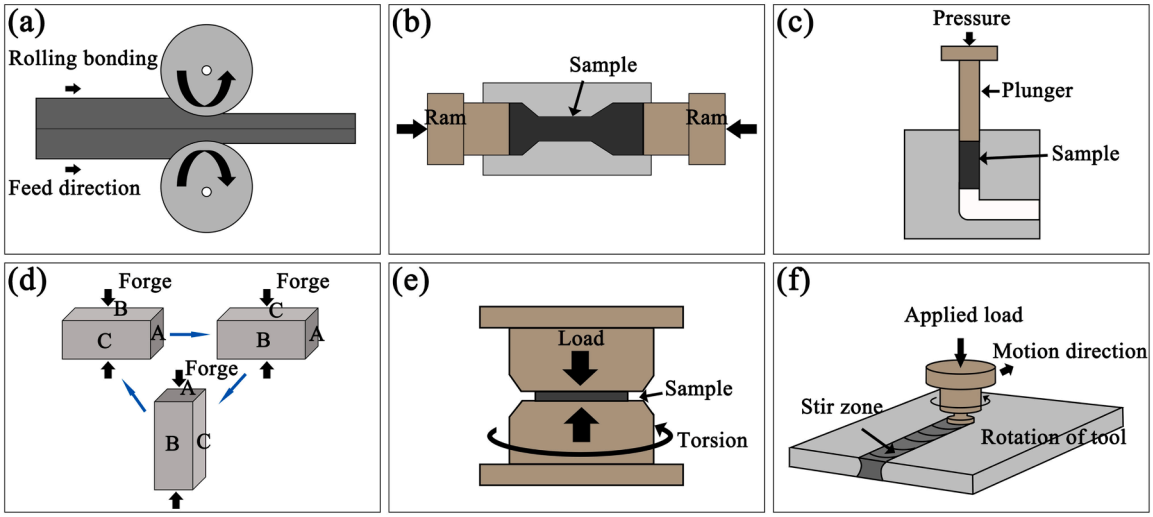

Fig. 3. Schematic diagrams of some SPD methods: (a) ARB, (b) CEC, (c) ECAP, (d) MDF, (e) HPT, (f) FSP.

highest yield strength (YS) and ultimate tensile strength (UTS) of 650 MPa and 710 MPa, respectively, comparable to high strength Al alloys and stainless steels [49]. After surveying the literatures, it is noticed that successful SPD processing of Mg alloys is very much temperature dependent. In order to impose high strains to Mg alloys without premature failure, the deformation temperature has to be increased to activate recrystallization and grain growth to certain extents. As a result, the grain sizes of many Mg alloys are hardly refined to the ultrafine grained regime. There is a limited number of reports on nanocrystalline Mg alloys with the average grain size below 100 nm, which are prepared by ball milling, surface nanocrystallization and HPT techniques [87, 111–113]. However, they are in the form of powders, films and thin sheets.

The strength vs. ductility data from Table 1 are plotted in Fig. 4a. It is clear that Mg alloys with different compositions and grain sizes demonstrate the "banana-shape" mutually exclusive relationship between strength and ductility. The majority of the deformed Mg alloys have the UTS below 500 MPa. In contrast, the UTS of Mg-Al and Mg-RE alloys prepared by RS and Mg-RE alloys prepared by FSP process are above 500 MPa. Only the strength of the Mg-RE alloys prepared by RS exceed 600 MPa. Li et al. [101] performed single-pass FSP and subsequent aging at 498 K to the Mg-Gd-Y-Zn-Zr alloy to achieve the YS of 401 MPa, UTS of 522 MPa and elongation to failure (EF) of 6.2 %. Chen et al. [105] prepared the gradient nanostructured AZ31B alloy rod with the YS of 491 MPa, UTS of 539 MPa and EF of 7.1 %, via 5-pass RS process. Chen et al. [106] prepared a high-strength AZ31 alloy rod with the YS of 488 MPa, UTS of 531 MPa and EF of 6.6 % by RS. Chen et al. [109] prepared Mg-Y-Zn alloy with the YS of 454 MPa, UTS of 509 MPa and EF of 5.4 % by RS. Huang et al. [110] performed RS and subsequent aging treatment to obtain the WE43 Mg alloy with the YS of 477 MPa, UTS of 516 MPa and EF of 8.5 %. However, the to-date record high strength for the Mg alloy was set by Wan et al. [49]. They obtained the high-strength Mg-Gd-Y-Zr alloy with the YS of 560 MPa, UTS of 630 MPa, EF of 5 % by RS process, and the YS and UTS of the RS sample were further improved to 650 MPa and 710 MPa after aging treatment, despite the declined EF to 4.5 %.

Fig. 4b shows the Hall-Petch relationship based on the data from Table 1. While the Mg alloys have very large varieties in terms of composition and microstructure, the data points agglomerate into two groups. The group of data set on the left-hand side of Fig. 4b indicates high lattice frictions and limited grain refinement; The group of data set on the right-hand side of Fig. 4b indicates low lattice frictions and large potential for grain refinement. The ARB and RS processes are very effective for achieving grain refinement in Mg alloys. Despite of significant grain refinement to near nanocrystalline regime achieved by the ARB process, the strength of the Mg-Li alloy is still below 200 MPa. For the Mg-Al and Mg-RE alloys, the YS are improved significantly when grain sizes are refined to the nanocrystalline regime. Most of the Mg alloys have the grain sizes above 1 μm even after SPD processing. The smallest average grain size achievable is still larger than 70 nm.

Since 2020, bulk nanocrystalline Mg alloys in the true sense have been successfully prepared using the RS method [49]. Fig. 5 shows a schematic diagram of the RS process. RS is a near-net forming process which uses multiple hammerheads to impact solid shaft or hollow tubes to reduced cross-sectional areas with high-frequency pulse loading [114–116]. RS imposes high strain rates (up to 100 s^{-1}) and three-dimensional distributions of complex stress and strain states, and thus are very effective for achieving grain refinement in Mg alloys. In addition, RS has the advantages of high-quality surface finish, low wastage and low cost. The equivalent strain of the round bars deformed by RS can be calculated by the following equation [114]:

$$\varepsilon = \ln\frac{S_0}{S_1} \tag{3}$$

where S_0 and S_1 are the initial and final cross-sectional areas, respectively.

In 2020, Wan and Zhao et al. obtained Mg-Gd-Y-Zr alloys with an average grain size of 80 nm by RS process, and the nanocrystalline samples were Φ3mm× 1000 mm rods with the YS up to 650 MPa, as shown in Fig. 6a-c [49]. During RS at room temperature, the Mg-Gd-Y-Zr alloy underwent the complex grain refinement process. At the early stage of plastic deformation, mechanical twins, mostly 86.7° tensile twins, subdivided the coarse grains into ultrafine platelets, as shown in Fig. 6d; As the plastic deformation proceeded to higher strains, dislocations accumulated into walls and low angle boundaries to subdivide the twin platelets into finer sub-grain bands (Fig. 6e); At the same time, in the non-twinned regions, band structures were formed by mutual trapping of dislocations and evolution of dense dislocation walls to sub-GBs, as shown in Fig. 6f and g. In the final stage, extensive SFs on basal plane and dislocation arrays divided the ultrafine grains into nano-domains; Dislocations accumulated on the SFs, causing the SFs to bend and eventually become HAGBs delineating the nano-grains, as shown in Fig. 6h and i.

In 2022, Chen et al. [106] processed the Φ16 mm rods of AZ31 and Mg-2Y alloys with the average grain sizes of 93 nm and 98 nm, respectively, by RS process. In 2023, Chen et al. [117] processed the AZ31B alloy by RS at cryogenic and room temperature. In both ways, they obtained bulk nanocrystalline Mg alloys, as shown in Fig. 7.

Table 1
A list of materials properties and grain sizes for Mg alloys processed by different plastic deformation methods including ARB, CEC, ECAP, MDF, HPT, FSP and RS.

Process	Material	Grain size (μm)	YS (MPa)	UTS (MPa)	EF (%)	Dimension	Ref.
ARB	Mg−8Li−3Al−1Zn	3	180	287.02	12.5	1.2 mm sheet	[51]
	Mg−5Li−1Al	0.1	195	318	8.43	1 mm sheet	[52]
	AZ31	38.2	222.8	295.4	6	2 mm sheet	[53]
	Mg−3Gd	0.182	253	265	4	1 mm sheet	[54]
	Mg−3Gd	0.2	285	300	2.8	1 mm sheet	[55]
	Mg−3Gd	3.3	173	214	36.6	1 mm sheet	[56]
CEC	Mg−1.5Zn−0.25Gd	3.4	161	251	31.4	Φ20 × 91 mm	[57]
	Mg−9.95Gd−2.3Y−0.46Zr	1.5	318	355	16.8	Φ20 * 91 mm	[58]
ECAP	Mg−9Li	1.6	149	187	42	20 × 20 × 40 mm^3	[59]
	Mg−8.4Li	24.4	175	186	16	10 × 10 × 60 mm^3	[60]
	Mg−8.4Li−3(Al−12Si)−1(Al−5Ti−1B)	22.5	170	243	16.7		
	Mg−8.4Li−3.58Al−0.36Si−0.05Ti−0.01B	6.52	167.7	263.4	9.9	10 × 10 × 60 mm^3	[61]
		20	170.6	242.8	16.8		
	AZ31	9–10	189	283	19.4	1.8 × 200 × 200 mm^3	[62]
	Mg−3.5Al−4.5Ca−0.4Mn	2.1, 10.9	275	331	7.4	20 × 20 × 45 mm^3	[63]
	Mg-Al-Ca-Mn	1.5	275	372	8	20 × 20 × 45 mm^3	[64]
	Mg−3.66Al−4.25Ca−0.43Mn	2.4	300	347	16	50 × 50 × 100 mm^3	[65]
	Mg−13Al	0.79	367	386	3.6	20 × 20 × 45 mm^3	[66]
	Mg−3.7Al−1.8Ca−0.4Mn	2.6	343	373	16.1	50 × 50 × 100 mm^3	[67]
	EZ33A	0.1–2, 20	327	346	4.1	Φ12 mm	[68]
	Mg−6.52Zn−0.95Y	2.9	290	385	22	20 × 20 × 70 mm^3	[69]
	ZE41A	0.5–2, 10–20	321	336	6.2	Cross section 10 × 10 mm^2	[70]
	Mg−0.6Zn−0.5Ca	1.5	372	375	7	Φ12 × 120 mm	[71]
	Mg−6.0Zn−0.5Ca−0.3Mn	1	269.6	323.9	22.7	10 × 10 × 70 mm^3	[72]
	Mg-Zn-Nd	10	213	240	32	Φ10 × 100 mm	[73]
	Mg-Gd-Zn-Zr	—	330	418	7.5	10 × 10 × 50 mm^3	[74]
	Mg−2.9Gd−1.5Nd−0.3Zn−0.3Zr	1.23	231.4	274.1	20.3	12 × 12 × 80 mm^3	[75]
	E675	1	345	365	22	15 × 15 × 120 mm^3	[76]
	Mg−5Y	1.24	273.9	306.4	23.9	20 × 20 × 70 mm^3	[77]
	Mg−2.9Gd−1.5Nd−0.3Zn−0.3Zr	< 2	210.9	263.9	27.9	12 × 12 × 80 mm^3	[78]
MDF	Mg−6.4Li−3.6Zn−0.37Al−0.36Y	10.8	150	207.5	38	cube	[79]
	AZ31	3.0–3.9	201	293	24.8	cube	[80]
	AZ80	—	343	430	11.4	100 × 100 × 140 mm^3	[81]
	E675	—	306	354	3.3	cube	[82]
	Mg−8.2Gd−3.8Y−1Zn−0.4Zr	0.9	417	434	12.9	billet	[83]
	Mg−5.95Gd−3.21Y−0.83Zn−0.32Ag−0.44Zr	2.91	295	364	4.8	160 × 260 × 460 mm^3	[84]
	Mg−8Gd−1Er−1Zn−0.6Zr	5.5	302.4	370.3	11.8	cube	[85]
HPT	Mg−6.2Zn−0.5Zr−0.2Ca	0.77	235	328	26.1	Φ10 × 0.8	[86]
		0.98	213	317	21.8	mm	
	Mg−4.7Y−4.6Gd−0.3Zr	—	450	475	2.5	Φ20 mm disk	[87]
		—	335	375	5.5		
FSP	Mg−10.05Li−2.85Al−3.07Zn−0.32Si	7.5	164	294	31	—	[88]
	LA103Z	8.1	285.9	305.5	4.05	—	[89]
	Mg−5Al−3.5Ca−1Mn	4.5	322	361	16	—	[90]
	AZ91	5	149	244	21	—	[91]
	ZKX50	0.8–1.2	146	247.9	15.7	—	[92]
	Mg−6Zn−1Y−0.5Zr	1.65	170	300	27	—	[93]
		3.58	140	280	28		
	Mg−6Zn−1Y−0.5Zr	2.1	170	310	27.7	—	[94]
	Mg−6Zn	3.6	133	280	18.6		
	Mg−1Zn−2Dy	3	120	242	28	—	[95]
	Mg-Mn-Ce	9	41	115	64	—	[96]
	Mg−4.27Y−2.94Nd−0.51Zr	2.7	290	303	11	—	[97]
	Mg−14Gd−0.4Zr	—	206	301	15	—	[98]
	WE43	2.1	233	350	16	—	[99]
	Mg−2Nd−0.2Zn	2	62	150	27.3	—	[100]
	Mg−13Gd−4Y−2Zn−0.6Zr	—	401	522	6.2	—	[101]
	Mg−10Gd−0.2Zr	5.78	202	272	7.5	—	[102]
	Mg−14Gd−2.5Zn−0.5Zr	< 2	289	343	13.3	—	[103]
RS	Mg−4Li−3Al−3Zn	—	360	405	5	Φ17.2 mm rod	[104]
	AZ31B	0.093	491	539	7.1	Φ3 mm rod	[105]

(*continued on next page*)

Table 1 (*continued*)

Process	Material	Grain size (μm)	YS (MPa)	UTS (MPa)	EF (%)	Dimension	Ref.
			463	507	10.5	Φ6 mm rod	
	AZ31	0.093	488	531	6.6	Φ16 mm rod	[106]
	ZK60	2.3, 14.1	200	341	27.6	Φ86.5 mm rod	[107]
	Mg−0.6Mn−0.5Al−0.5Zn−0.4Ca	1.41	403	427	9.1	Φ14 mm rod	[108]
	Mg−8Gd−3Y−0.4Zr	0.080	560	630	5	Φ3 * 1000	[49]
			650	710	4.5	mm	
	Mg−3.16Y−1.87Zn	0.107	454	509	5.4	Φ16 mm rod	[109]
		0.116	398	470	11.5		
	WE43	0.081	477	516	8.5	Φ15.6 mm rod	[110]
	Mg−2Y	0.098	339	395	10.7	Φ16 mm rod	[106]

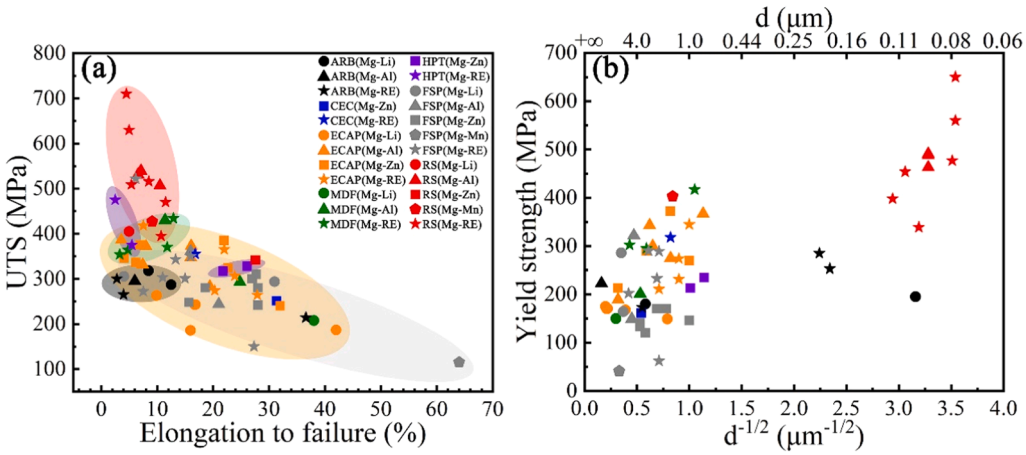

Fig. 4. (a) Comparison of UTS and EF for various Mg alloys prepared by different SPD techniques. (b) A compilation of the tensile YS as a function of grain size of various Mg alloys produced by different SPD techniques. The upper x-axis is the grain size, which corresponds to the lower x-axis $d^{-1/2}$.

Nevertheless, the cryogenic RS has a better grain refinement effect than the room temperature RS. Under the combined action of high strain rate and low temperature, deformation twinning in multiple systems (tensile twins in dominance) are activated. Deformation twins intersect one another to divide the coarse grains into lamellar structures. With the increasing strain, sub-grains formed at twinning intersections and inside twin bands. Eventually, the dynamic balance between grain refinement and recrystallization, resulting in nanograins with random orientations. The grain refinement mechanism of the AZ31B alloy during cryogenic RS is shown in Fig. 8 [117]. Recently, Yang and Zhao et al. [104] for the first time used a low-strain RS treatment to prepare ultra-strong bulk Mg-Li alloys, as shown in Fig. 9a and b. The RS Mg-Li samples were Φ17.2 mm rods. The core region of the rod has the UTS of 368 MPa, as shown in Fig. 9a, and the peripheral region of the rod has the UTS of 405 MPa. The RS Mg-Li alloy has high densities of SFs and twins as shown in Fig. 9c-f.

Jian et al. [118] used conventional hot rolling to introduce high densities of SFs in Mg-8.5Gd-2.3Y-1.8Ag-0.4Zr alloy. The hot rolled Mg alloy has a YS of 575 MPa, UTS of 600 MPa, and uniform elongation of 5.2 %, as shown in Fig. 10. It can be seen that the material strength is significantly improved as the spacing of SFs decreased to a few tens of nanometers. Apparently, twins and SFs play indispensable roles for strengthening Mg alloys, and the strength increments can be calculated by the equation [104,119]:

$$\Delta\sigma = m(k_1\lambda^{-1/2} + k_2 d^{-1}) \quad (4)$$

where λ is the average thickness of twin bands; d is the average spacing of SFs; m is the volume fraction of twins or SFs, k_1 is the Hall Petch constant, k_2 is an experimental constant.

In summary, the grain refinement effects imposed by conventional plastic deformation and SPD to Mg alloys are sensitive to the compositions of alloys and deformation temperatures; nonetheless, grain refinement to nanocrystalline regime is still a challenge. Before 2020, the nanocrystalline Mg alloys are limited to powder, film and thin sheets; In order to achieve ultrafine grains and/or nano-grains in Mg alloys, complex processing routes and the associated high preparation cost are required. Since 2020, RS treatment has been done to a large variety of Mg alloys, demonstrating a new route for large-scale low-cost preparation of bulk nanocrystalline Mg alloys.

3.2. *Solid solution and precipitation strengthening via addition of RE elements*

Solid solution and precipitation strengthening are realized by adding controlled amounts of alloying elements to Mg alloys. Especially the RE elements pose significant effects to strengthen the Mg alloys, because RE elements have large atomic sizes and high solubility in Mg. The solute atoms and precipitates create barriers against dislocation slip in the Mg alloys [120]. Influenced by the solid solubility of RE elements in the Mg matrix, the YS of coarse-grained Mg-RE alloy is close to 400 MPa [121–123].

3.2.1. *Solution strengthening*

Adding solute atoms to the Mg matrix causes lattice distortions to some extent, increases the energy barrier against dislocation slip, and thus increases the strength. This phenomenon is called solution strengthening. Yasi et al. [124] constructed a mesoscale model for predicting solute strengthening in Mg alloys based on first principles calculations. As shown in Fig. 11a, the solid solution strengthening effects of 29 alloying elements in Mg are presented. The solid solution strengthening effect can be estimated by the equation [49,125]:

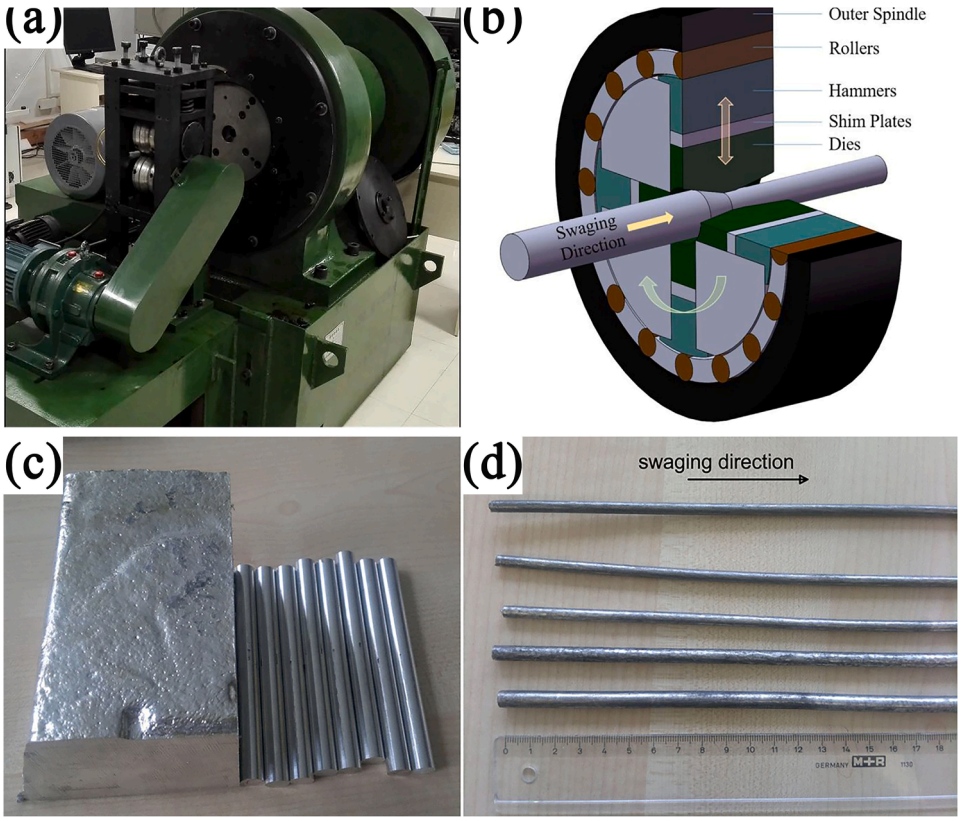

Fig. 5. (a) A photo of a RS machine [114]; (b) The operational principle of RS [115]; (c) As-received Mg ingot and rods [116]; (d) The Mg rods after RS treatment [116]. Reproduced with permissions from Ref. [114–116].

$$\sigma_s = \sigma_y + \frac{3.1\varepsilon G C^{1/2}}{700} \tag{5}$$

Where σ_y is the YS of pure Mg, ε is an experimental constant, G is the shear modulus, C is the solute concentration in atomic percentage.

Kula et al. [126] found that the critical resolved shear stress (CRSS) of all slip systems in Mg increased monotonically with the increase of Y concentration, but the rate of increase was different. Y addition can significantly increase the CRSS for <c + a> slip. The contribution of solid solution strengthening to the yield stress of a bulk Mg alloy is closely related to the CRSS of basal slip. Gao et al. [125] found that the YS of Mg-Gd, Mg-Y and Mg-Gd-Y alloys is strongly related to the concentration of Gd and Y elements; The solid solution strengthening effects of Gd and Y are much larger than that of Al and Zn. Fig. 11b shows the mechanical properties of Mg-Gd alloys with different Gd contents. With the increase of Gd in concentration, YS and UTS of the Mg-Gd alloys increase, but their plasticity decreases. Kim et al. [127] found that when the content of Gd was increased from 1 wt% to 10 wt%, the YS of Mg-Gd binary alloy increased almost linearly, from 94 to 159 MPa, due to solid solution strengthening. In addition, Mo et al. [128] used atom probe tomography (APT) analysis and atomic-resolution high-angle annular dark field scanning transmission electron microscopy (HAADF-STEM) to verify for the first time that Gd and Ca in Mg have the strong tendency for co-cluster formation, and the Gd-Ca co-clusters with short-rang orders can provide significant solid solution strengthening effect.

3.2.2. *Precipitation strengthening*

Precipitation strengthening is a convenient and effective strengthening method, which is suitable for industrial applications. The shape, quantity and distribution of precipitates are the main factors that determine the precipitation strengthening effect. Dislocation-precipitate interactions are governed by two mechanisms: the Orowan bypass mechanism and shearing mechanism. Fig. 12a presents a schematic diagram of the Orowan bypass mechanism. When a gliding dislocation encounters a hard and non-deformable particle, the dislocation bends and eventually bypasses the particle under the applied stress, and leaving a dislocation loop around the particle. The strengthening contribution of the Orowan bypass mechanism can be calculated by the following equation [129]:

$$\Delta\tau = \frac{Gb}{2\pi\lambda\sqrt{1-\nu}}\ln\frac{d_p}{r_0} \tag{6}$$

where $\Delta\tau$ is critical shear stress, G is the shear modulus, b is magnitude of the Burgers vector of the gliding dislocation, λ is the effective planar interparticle spacing, ν is Poisson's ratio, d_p is the mean planar diameter of the particles and r_0 is the core radius of the dislocation. Recently, Xu et al. [129] observed that <a> dislocations squashed into the interface and bowed out to bypass the β' phase in the Mg-10Gd alloy by using an in-situ TEM technique. The result supports Orowan mechanism as the main strengthening mechanism in Mg-Gd alloys.

When a dislocation encounters a particle which is comparatively soft and semi-coherent to the matrix, the dislocation can shear through the particle and continue to slip via the shearing mechanism, as shown in Fig. 12b. The strengthening effect by the shearing mechanism can be calculated by the equation [130]:

$$\Delta\tau = BG\varepsilon^{3/2}\sqrt{\frac{fr}{b}} \tag{7}$$

where B is a constant, G is the shear modulus, ε is the misfit strain, f is the volume fraction of particles, and r is the mean radius of the particles. Jiang et al. [131] studied Mg-Zn-Mn alloys by means of high-resolution TEM and found the shear trace lines left after that <c + a> dislocations sheared through (0001) precipitates.

The strength of the Mg-Li binary alloy is very low. Al or Zn are

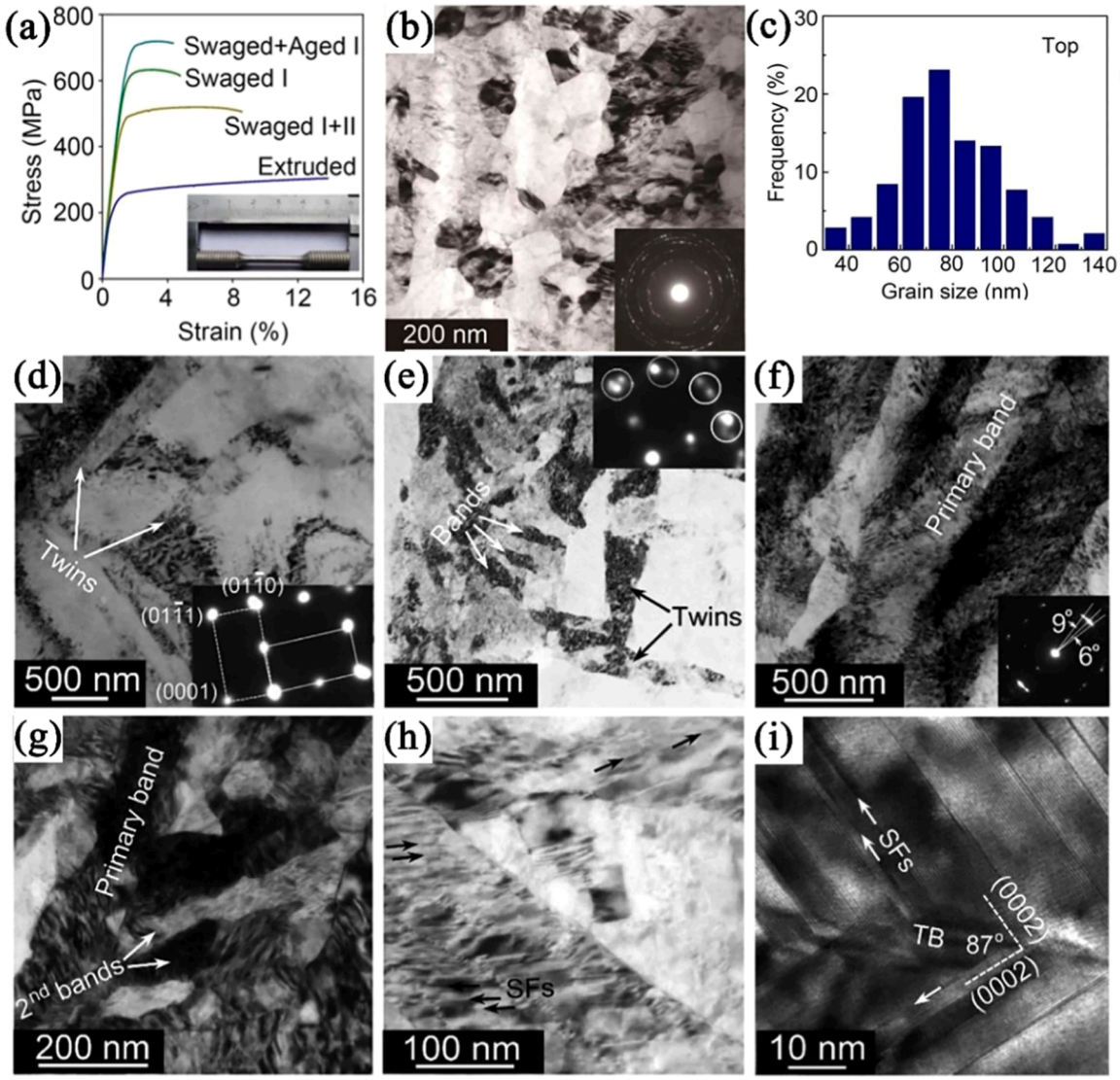

Fig. 6. Mechanical properties, microstructure and grain refinement mechanisms for the RS Mg-Gd-Y-Zr alloy. (a) Tensile properties; (b) Bright-field TEM image showing ultrafine/nano grains in the RS Mg-Gd-Y-Zr alloy; (c) Grain size distribution chart for the RS Mg-Gd-Y-Zr alloy; (d) At 6 % RS strain, $\{10\bar{1}2\}$ tension twins were produced; (e) At 16 % RS strain, the twins were segmented into smaller sub-grain bands, and the selected area electron diffraction (SAED) pattern revealed LAGBs; (f) At 6 % RS strain, numerous primary deformation bands were observed in the twin-free regions, and the SAED pattern revealed LAGBs; (g) At 16 % RS strain, dislocation arrays divided the primary bands; (h, i) At 26 % RS strain, a series of SFs were observed [49]. Reproduced with permission from Ref. [49].

usually added to the Mg-Li based alloys for precipitation strengthening. For example, Park et al. [132] added different amounts of Al to the Mg-15Li alloy to make lightweight and high-strength Mg-Li-Al alloys. The compressive YS of the alloy increased and the density of the alloy decreased slightly with the increasing content of Al. Ji et al. [133] reported that precipitation of the semi-coherent $(Mg, Li)_3Zn$ phase is responsible for the rapid age hardening of the Mg-10Li-5Zn alloys. High densities of $Mg_{17}Al_{12}$ precipitates in the form of platelets on basal planes are observed in the AZ80 Mg alloy, as shown in Fig. 13 [134]. When the matrix grain is oriented to $[0001]_\alpha$ zone axis, $Mg_{17}Al_{12}$ platelets are oriented to three $< 2\bar{1}\bar{1}0 >_\alpha // < 1\bar{1}\bar{1} >_\beta$ directions; When the matrix grain is oriented to $[10\bar{1}0]_\alpha$ direction, all $Mg_{17}Al_{12}$ platelets are parallel to the basal plane. Readers can refer to Celotto et al. [135] and Lai et al. [136] for detailed survey of the $Mg_{17}Al_{12}$ precipitates in Mg-Al alloys.

Conventional thermal aging processes can significantly improve the mechanical properties of many Al alloys, but in contrast the strengthening effect is very much limited in Mg alloys, because of the easy formation of coarse intermetallic particles and the sparse particle spacing. If the aging temperature is lowered, the growth of particles can be inhibited, but the peak aging time will become unacceptably long. Recently, Ma et al. [137] compared the dynamic precipitation and conventional aging precipitation of the Mg-9wt%Al alloy. A large number density of nano-precipitates with low aspect ratios were successfully made in the Mg-9wt%Al alloy via dynamic precipitation induced by warm ECAP, as shown in Fig. 14. Liu et al. [134] regulated the orientations of precipitates in the AZ80 Mg alloy to significantly increase the YS to 311 MPa. Rod-shape β_1' ($MgZn_2$) and plate-shape β_2' ($MgZn_2$) precipitates play the major roles in precipitation strengthening of Mg-Zn alloys. Li et al. [138] found that the CRSS for basal slip and extension twinning are increased due the formation of high densities of $MgZn_2$ precipitates in Mg-Zn alloys, while the CRSS for pyramidal slip was less affected. In addition, the solid solution strengthened Mg-Zn alloys have high anisotropy ratios which are significantly reduced in the precipitation strengthened Mg-Zn alloys. Zhou et al. [139] simultaneously improved the tensile strength and plasticity of the Mg-Zn alloy by low-temperature aging. The aged Mg-Zn alloy has the UTS of 232 MPa, YS of 89 MPa and EF of 11 %, which are 5.5 %, 12.7 %, and 22.2 % higher than that of the solution-treated alloy, respectively. For

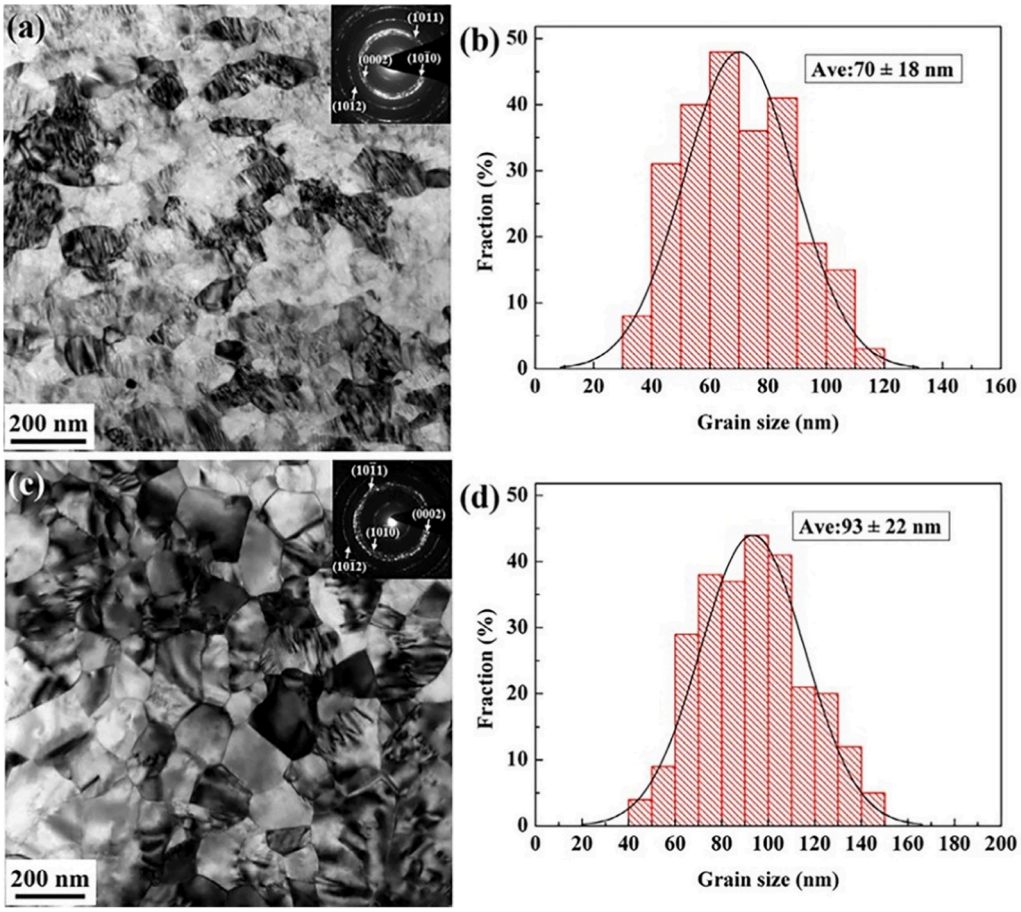

Fig. 7. Microstructure and grain sizes of the AZ31B alloy sample prepared via RS: (a, b) cryogenic deformation, (c, d) room temperature deformation [117]. Reproduced with permission from Ref. [117].

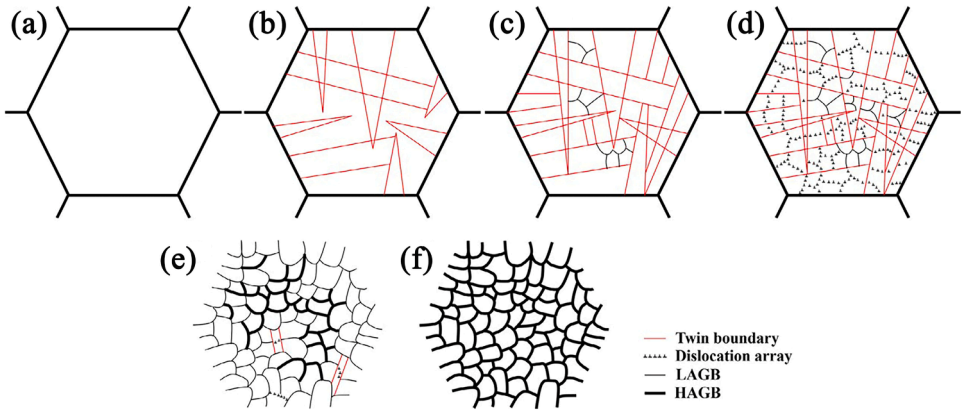

Fig. 8. Schematic diagram illustrating the grain refinement process of the AZ31B Mg alloy under cryogenic RS. (a) Undeformed grain; (b) Deformation twinning in multiple systems; (c) Twins and nanoscale sub-grains form at twin intersections; (d) Twin lamellae are subdivided by dislocation arrays; (e) Ultrafine sub-grains; (f) Homogeneous nano-grains [117]. Reproduced with permission from Ref. [117].

Mg-Mn binary alloys, the addition of Mn improves the ductility, but the YS is unsatisfactory. Recently, Peng et al. [140] added a small amount of Al to a Mg-Mn alloy to obtain a low cost, high strength and high ductility Mg-1Mn-0.5Al alloy. The Al_8Mn_5 particles in the Mg-1Mn-0.5Al alloy have a significant effect on the mechanical properties. The YS, UTS, EF of the Mg-1Mn-0.5Al alloy are 248 MPa, 263 MPa, and 33 %, respectively.

For many of the Mg-RE alloys, when the contents of RE elements are higher than 10 % in mass fraction, the precipitation strengthening effects become suddenly noticeable. Mg-Gd series alloys have remarkable age hardening effects. Adding Y, Nd, Zn, Li, etc. to Mg-Gd alloys can further improve the mechanical properties and reduce the cost. For example, Yu et al. [141] solved the ambient strength-ductility dilemma in Mg-Gd alloys via Li addition. As shown in the Fig. 15, the addition of Li boosted precipitation of β, β_{1R}, $\beta'_{H\text{-}II}$ phases with different sizes, and enhanced the activity of <c + a> dislocations. The Mg-Gd-Y series alloys developed by Rokhlin and Kamado et al. are representative high-performance Mg-RE alloys, and have been extensively studied in

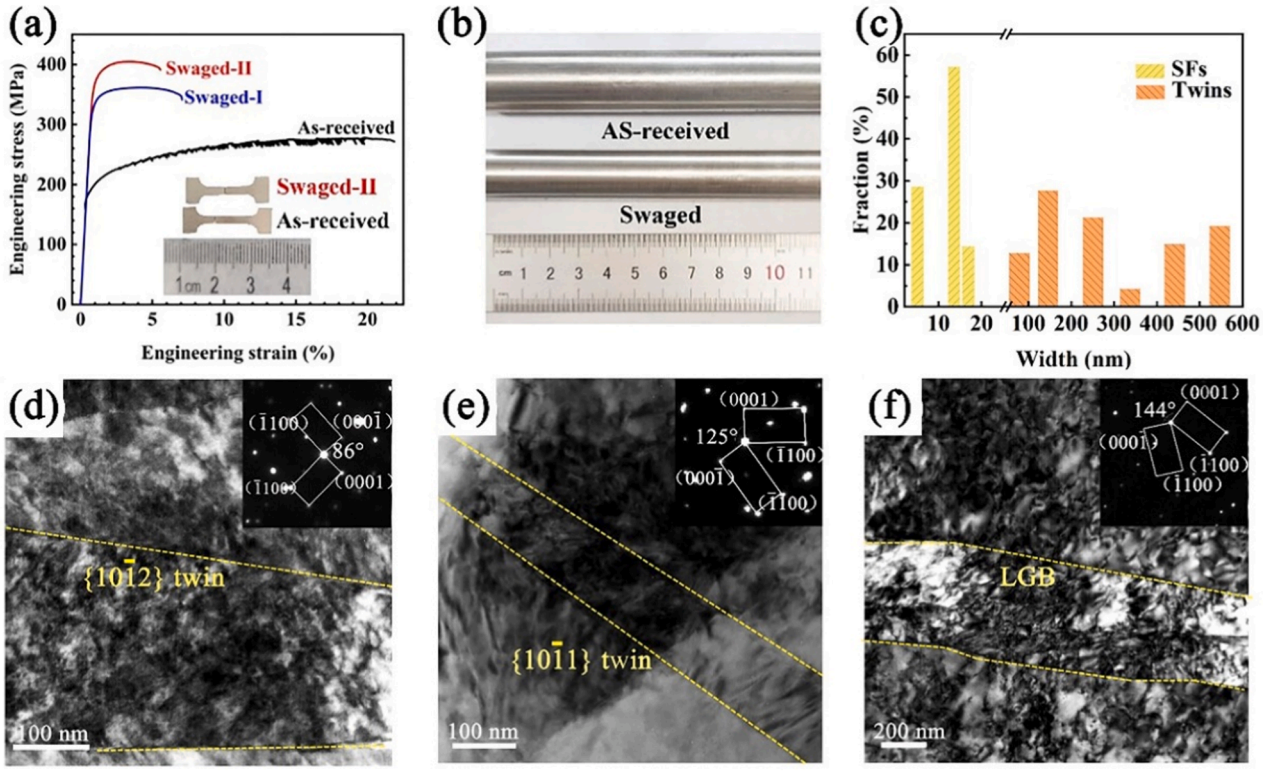

Fig. 9. Mechanical properties and microstructures of the RS Mg-Li alloys. (a) Tensile properties of the as-received and RS samples; (b) A photo of the as-received and RS samples; (c) Measured widths of twins and SFs; (d-f) TEM images of the RS Mg-Li alloy [104]. Reproduced with permission from Ref. [104].

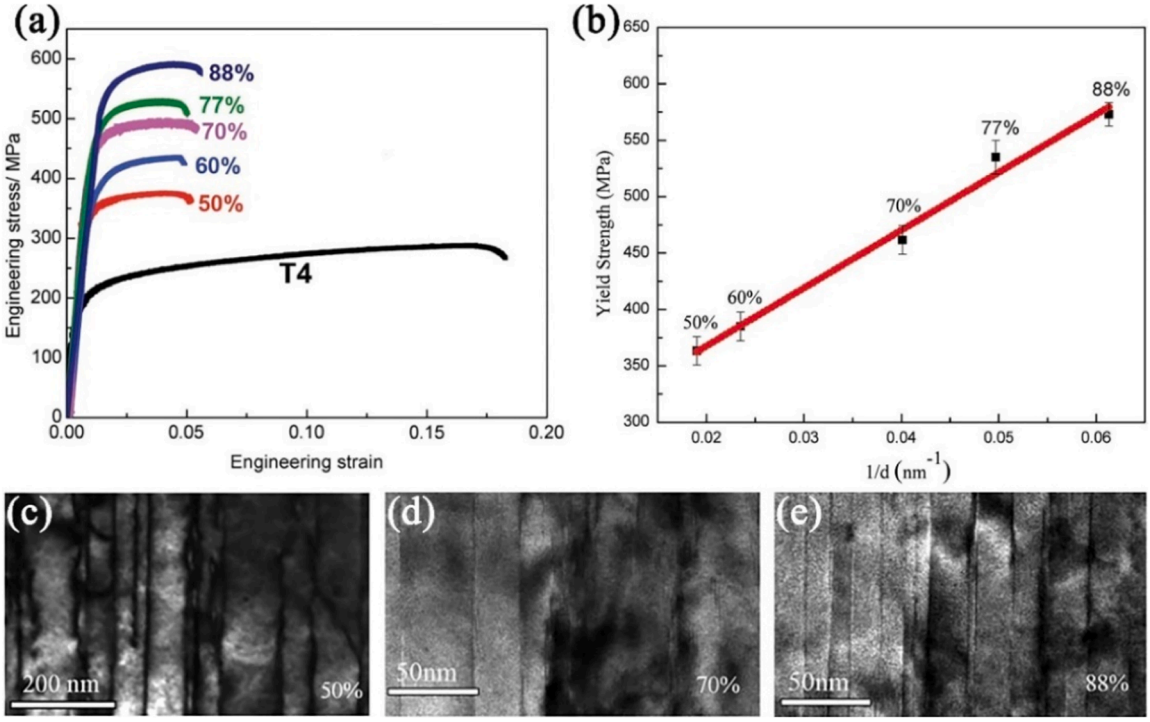

Fig. 10. (a) Tensile properties of the Mg-8.5Gd-2.3Y-1.8Ag-0.4Zr alloy subjected to heat treatment and hot rolling to different rolling reductions. (b) YS vs. the reciprocal of the mean spacing of SFs. TEM images showing SFs in the Mg alloy samples processed to different rolling reductions: (c) 50 %, d= 55 nm, (d) 70 %, d= 25 nm and (e) 88 %, d= 16 nm [118]. Reproduced with permission from Ref. [118].

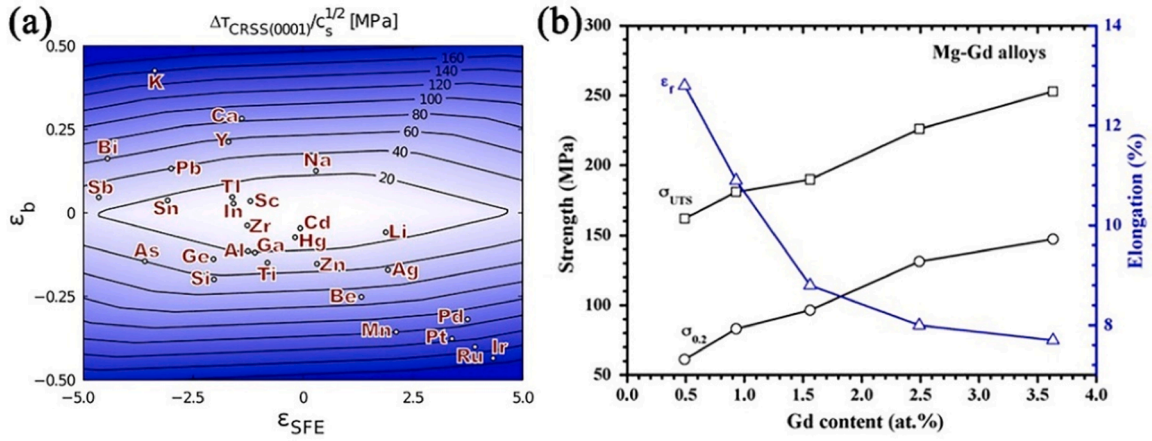

Fig. 11. (a) Solid-solution strengthening potency (contours) of 29 different solutes in Mg as a function of size and chemical misfits [124]; (b) Correlation between the tensile properties of Mg-Gd alloys and concentrations of solute atoms [125]. Reproduced with permissions from Ref. [124,125].

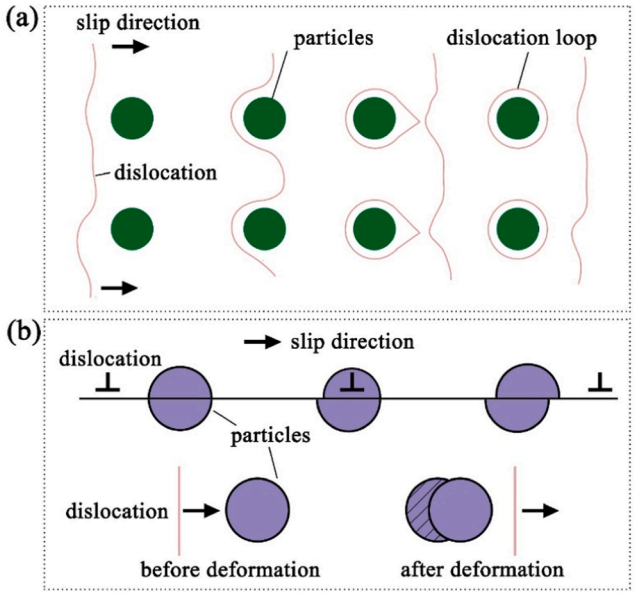

Fig. 12. Schematic diagrams of (a) the Orowan bypass mechanism and (b) shearing mechanism.

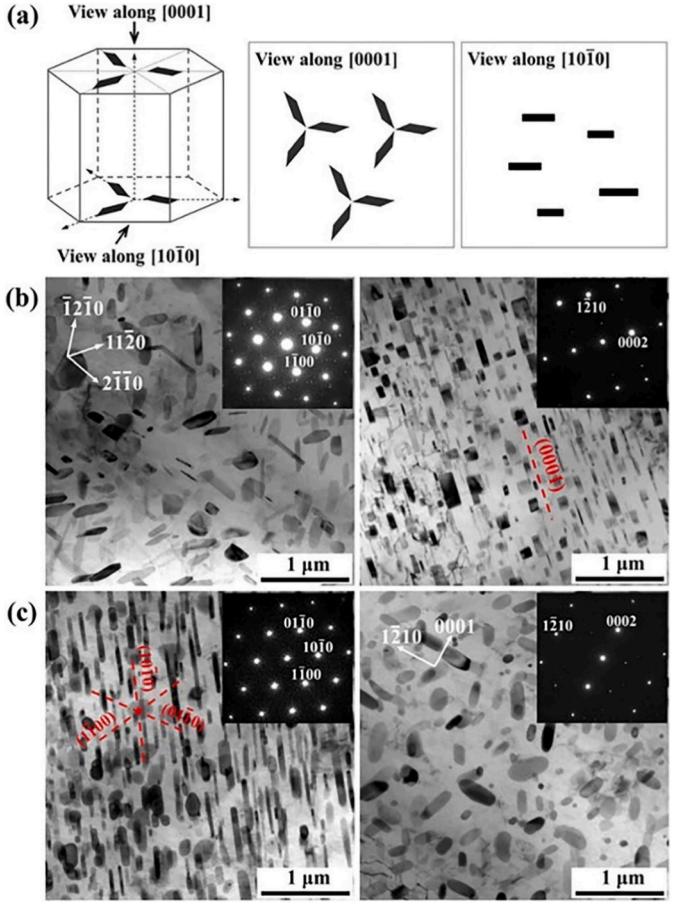

Fig. 13. (a) Schematic morphology of $Mg_{17}Al_{12}$ precipitates observed from the $[0001]_\alpha$ and $[10\bar{1}0]_\alpha$ zone axes; TEM images showing actual $Mg_{17}Al_{12}$ precipitates observed from the (b) $[0001]_\alpha$ and (c) $[10\bar{1}0]_\alpha$ zone axes, respectively [134]. Reproduced with permission from Ref. [134].

recent years [142,143]. It is found that adding Zn or Ag elements to Mg-Gd-Y alloy can further improve the precipitation strengthening effect [144]. Homma et al. [145] prepared an ultra-strong Mg-1.8Gd-1.8Y-0.7Zn-0.2Zr alloy with the UTS of 542 MPa, YS of 473 MPa and EF of 8.0 %. The high strength is attributed to precipitation of fine particles at the boundaries of dynamically recrystallized grains, as shown in Fig. 16. Moreover, Wang et al. [146] added Ag to the Mg-Gd-Y alloy to obtain an ultra-strong Mg-RE alloy. After aging treatment, the YS, UTS and EF of the as-cast Mg-Gd-Y-Ag alloy at room temperature were 268 MPa, 403 MPa and 4.9 %, respectively. Zhou et al. [147] revealed the effects of Ag on segregation at twin boundaries, SFs and GBs in the Mg-Gd-Y alloys using atomic-resolution HAADF--STEM imaging and EDS mapping.

In recent years, many scientific research teams have carried out research work on the phase diagram, grain refinement, deformation behavior, dynamic recrystallization, strengthening mechanism and other aspects of Mg-Gd-Y alloys [148–152]. For example, He et al. [153, 154] systematically studied precipitation dynamics in Mg-Gd and Mg-Gd-Y alloys at different aging stages, and found the precipitation sequence of super-saturated solid solution (S.S.S.S.) → β'' → β' → β_1 → β.

β' has the base-centered orthorhombic (BCO) crystal structure, and is the major beneficial precipitate for strengthening the Mg alloys. The β' precipitate is formed via ordered substitution of Mg atoms by RE atoms. The β' precipitates show convex lens shapes. The β' precipitates have the long axes parallel to $\{11\bar{2}0\}_\alpha$ planes and thus perpendicular to the $(0001)_\alpha$ basal planes, creating closely spaced interfaces to block

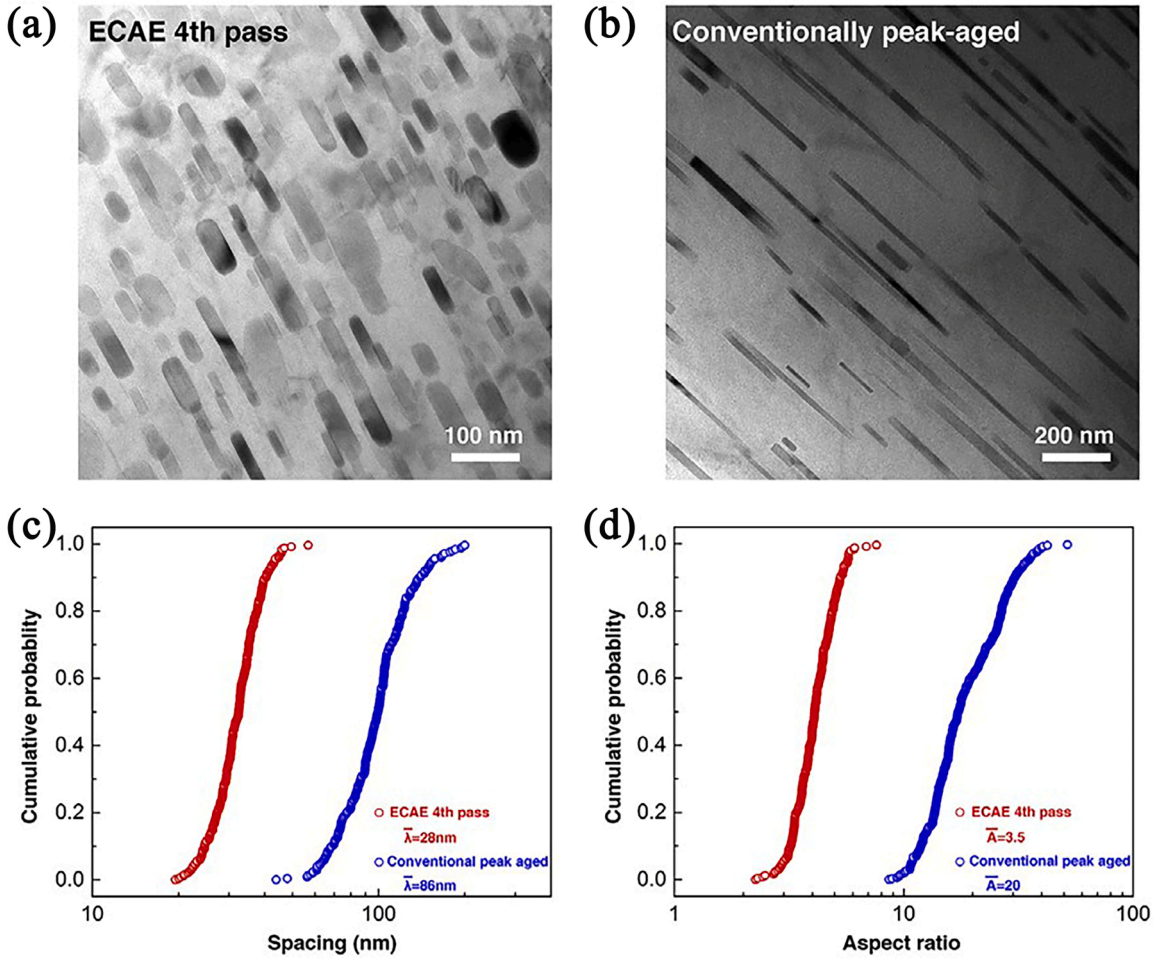

Fig. 14. TEM images showing precipitates in (a) the warm-ECAP Mg-9wt%Al sample, and (b) statically peak-aged Mg-9wt%Al sample (both images were obtained at $< 11\bar{2}0 >$ zone axis); (c) Spacing of precipitates; (d) Aspect ratios of precipitates [137]. Reproduced with permission from Ref. [137].

dislocation slip on basal planes. Provided that the main slip systems in Mg alloys at room temperature are the basal slip systems, the mechanical properties can be significantly improved with increasing volume fraction, density and aspect ratios of the β' precipitates [155].

Adding Zn to Mg-Y alloys can form precipitates with long period stacking ordered (LPSO) structures which can be further derived into 10 H, 14 H, 18 R, and 24 R structures [156–162]. Fig. 17 [159] shows electron diffraction patterns of LPSO structures in some Mg-Zn-RE alloys. The formation of LPSO structures is strongly affected by the thermal history and shear strain fields. The precipitates with LPSO structures are found to co-exist with the β' phase in the peak aged samples, and can improve the age strengthening effect for the Mg-Zn-RE alloys. Apparently, the lattice structure, micromorphology, compound type, size, distribution and density of the precipitates are all important factors that determine the precipitation strengthening effect.

Chen et al. [39] added 14 vol% of SiC nanoparticles into the Mg2Zn alloy, and then conducted HPT for grain refinement. The HPT processed nanostructured Mg2Zn alloy has the YS of 710 MPa. Wu et al. [38] prepared a 10 μm thick composite film having $MgCu_2$ particles with the sizes of ~6 nm embedded in the amorphous Mg matrix, by magnetron sputtering. The composite film shows the ultra-high stress of 3.5 GPa. The abovementioned Mg alloy-based composites are different from traditional Mg alloys. Note that the strength of the composites has been measured by micro-pillar compression tests which may be sensitive to the size effect. Another critical issue for the Mg alloy-based composites with ultra-high strength, is how to scale up the sample size.

4. Deformation mechanisms in Mg alloys and the various schemes to improve plasticity

4.1. Deformation mechanisms in Mg alloys

Fig. 18 shows a schematic diagram of HCP structure and the slip systems. The independent slip systems in HCP structure are listed in Table 2 [34,163]. Mg and Mg alloys with the HCP structure thus have basal, prismatic and pyramidal slip systems. In all available slip systems, <a> slip has the lowest CRSS, and thus easily activated. However, there are no more than four independent slip systems available for <a> slip. According to the von Mises criterion for homogeneous deformation, activation of at least five independent slip systems is needed. Therefore, <c + a> slip and/or deformation twinning are necessary to accommodate plastic strains in Mg alloys. However, the CRSS for twinning and <c + a> slip is significantly higher than <a> slip, leading to inhomogeneous deformation and even premature failure in Mg alloys especially for coarse grain Mg alloys.

Basal <a> dislocation, non-basal <c> and <c + a> dislocations are commonly observed in deformed Mg alloys. Non-basal <c + a> slip alone can provide five independent slip systems in Mg alloys, and most importantly to accommodate the strains along the c-axis. Therefore, the ductility of Mg alloys is strongly related to the activities of non-basal <c + a> dislocations. In other words, massive activation of non-basal <c + a> dislocations are the key to high ductility of Mg alloys. Liu et al. [164] conducted in-situ TEM compression tests to investigate <c + a> dislocation motions in Mg single-crystal pillars, as shown in

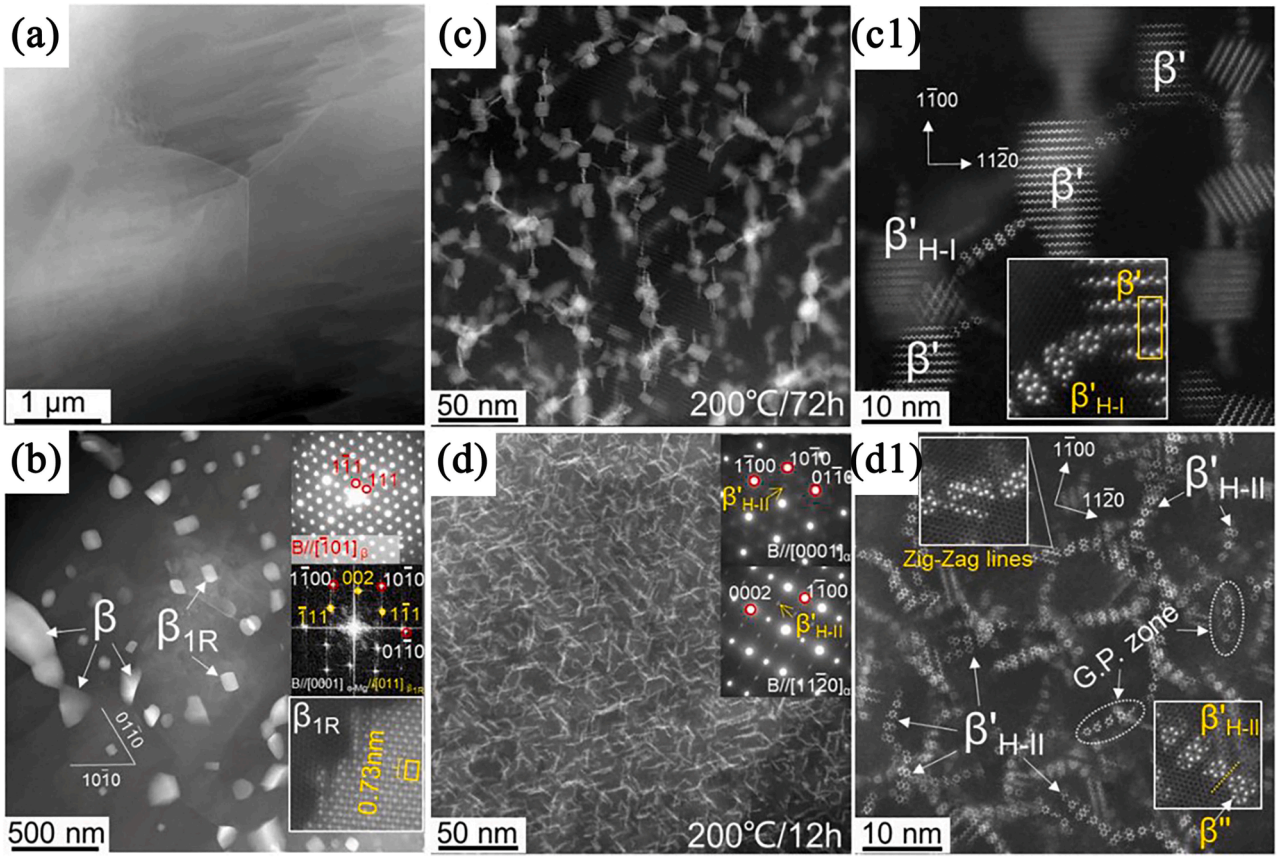

Fig. 15. HAADF-STEM images of (a) as-extruded 0Li alloy, (b) as-extruded 1Li alloy, (c, c1) peak-aged 0Li alloy, and (d, d1) peak-aged 1Li alloy [141]. Reproduced with permission from Ref. [141].

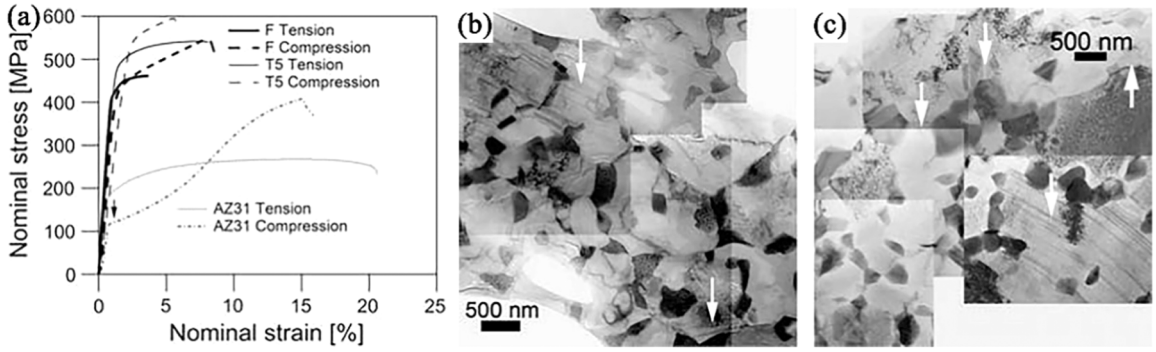

Fig. 16. (a) Mechanical properties of as-extruded and T5-aged samples under tension and compression; TEM images showing precipitates at GBs in the (b) as-extruded and (c) T5-aged samples [145]. Reproduced with permission from Ref. [145].

Fig. 19. There are literatures reporting that the non-basal <c + a> dislocation is metastable, and thus can easily dissociates [165]. There are two <c + a> dislocation decomposition mechanisms that have been proposed [166]: (1) As shown in Fig. 20a, a gliding <c + a> dislocation on a pyramidal plane dissociates into a sessile <c> dislocation and a glissile <a> dislocation in a cross-slip process; This decomposition is energetically favored. (2) As shown in Fig. 20b, a gliding <c + a> dislocation on a pyramidal plane may become unstable; Hence, a segment of the <c + a> dislocation (the purple segment) dissociates into the I1 SF enclosed by a leading partial and a trailing partial; Another segment of the <c + a> dislocation (the blue segment) dissociates into a sessile <c> dislocation and a glissile <a> dislocation which glides away on another slip plane. Curtin et al. [34] found that a <c + a> dislocation may undergo thermally activated and stress-dependent transition to one of three lower-energy basal-dissociated immobile dislocation structures, which exerts the strong blocking effect against the movement of other dislocations, resulting in the low plasticity of Mg.

While HCP Mg alloys have low lattice symmetry and an insufficient number of easy slip systems, deformation twinning is necessary to coordinate the plastic deformation, especially the strain along c-axis. Experimentally verified twinning systems in HCP Mg alloys are listed in Table 3 [167–171]. The main twin systems in Mg alloys are $\{10\bar{1}2\}$ tensile twins, $\{10\bar{1}1\}$ compressive twins and $\{10\bar{1}3\}$ twins. The generation and annihilation of deformation twins, and the segregation of solute atoms at twin boundaries have important effects on the mechanical properties of Mg and Mg alloys [172–174].

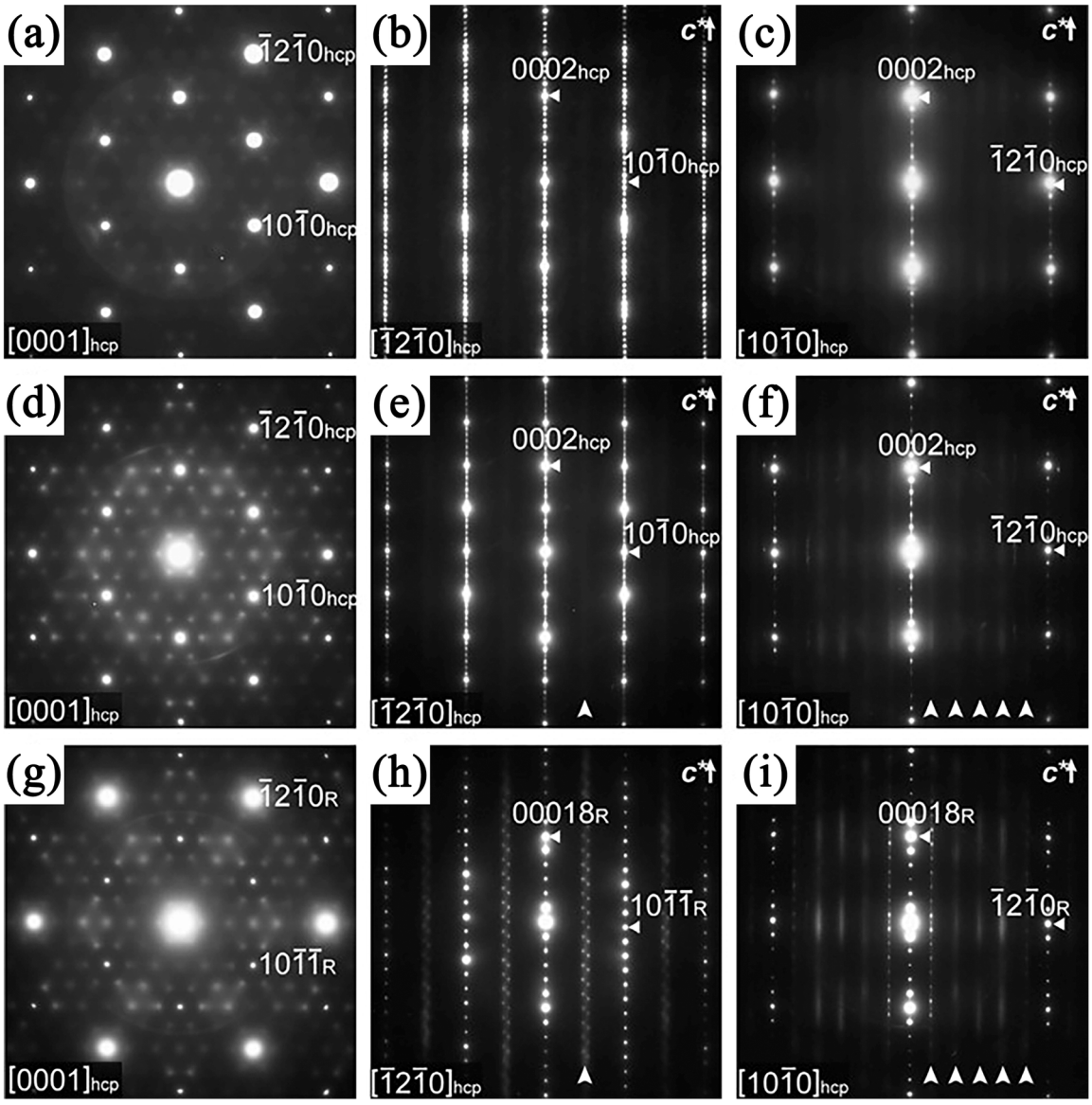

Fig. 17. Electron diffraction patterns of the LPSO phases in (a-c) $Mg_{97}Zn_1Y_2$, (d-f) $Mg_{97}Zn_1Er_2$, (g-i) $Mg_{85}Zn_6Y_9$ alloys [159]. Reproduced with permission from Ref. [159].

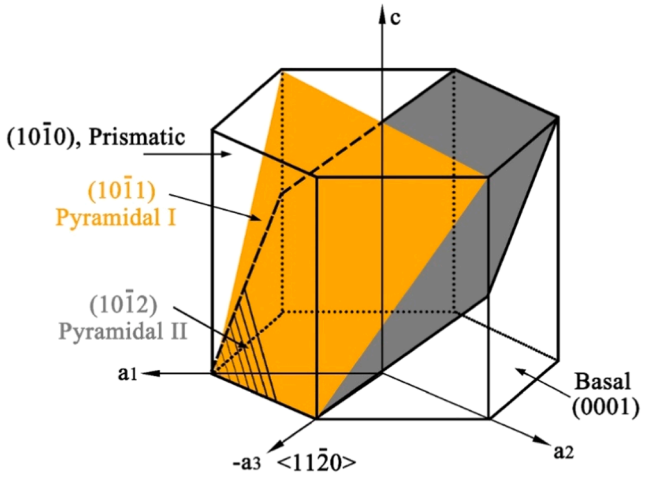

Fig. 18. A schematic diagram showing the HCP structure and slip systems.

Table 2
Independent slip systems in HCP Mg alloys [34,163].

Slip system	Slip plane	Slip direction		Number of independent slip system
Basal slip	{0001}	$< 11\bar{2}0 >$	<a>	2
Prismatic slip	{10$\bar{1}$0}	$< 11\bar{2}0 >$	<a>	2
	{10$\bar{1}$0}	$< 0001 >$	<c>	2
	{11$\bar{2}$0}			
Pyramidal slip	{10$\bar{1}$1}	$< 11\bar{2}0 >$	<a>	4
	{10$\bar{1}$1}	$< 11\bar{2}3 >$	<c + a>	5
	{11$\bar{2}$2}			

SFs are easily formed during the plastic deformation of Mg alloys. Different types of SFs in HCP Mg alloys are collected in Table 4 [175]. The generation of SFs is related to the slip motion of dislocations. The commonly observed SFs in Mg alloys are I1 and I2 faults. The I1 fault is also known as the solidified fault, and is formed by the collapse of vacancies or a vacancy loop. The I2 fault is commonly known as the deformation fault, which is formed by the decomposition of a full

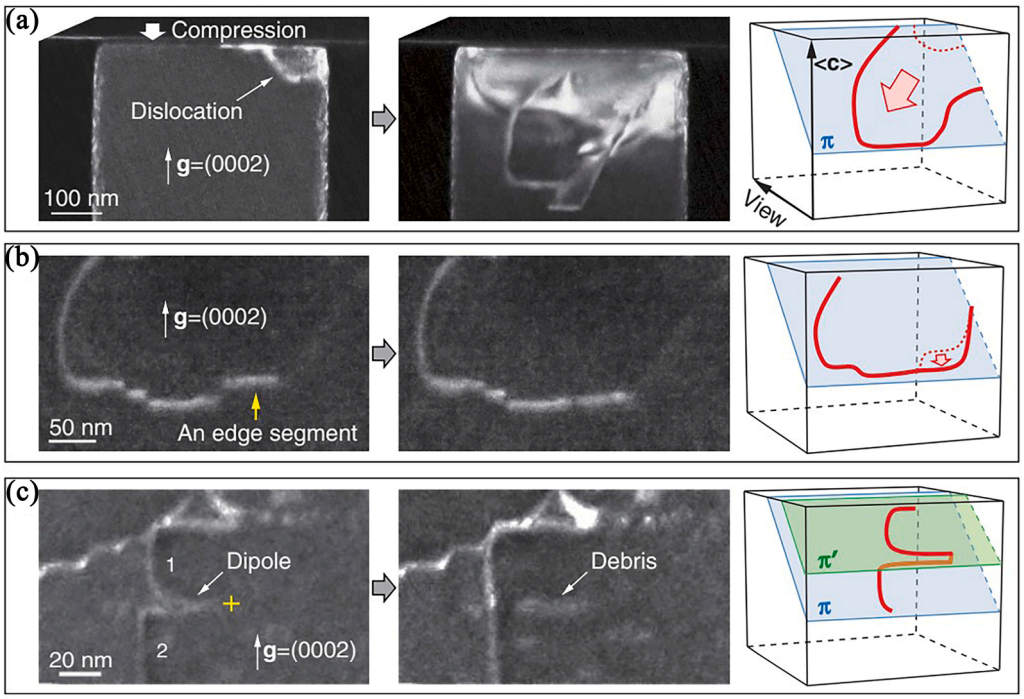

Fig. 19. TEM images and schematic diagrams illustrating <c + a> dislocations with different configurations and motion in Mg single-crystal pillars: (a) expansion of a half loop; (b) motion of an edge segment; (c) Formations of a dislocation dipole and debris [164]. Reproduced with permission from Ref. [164].

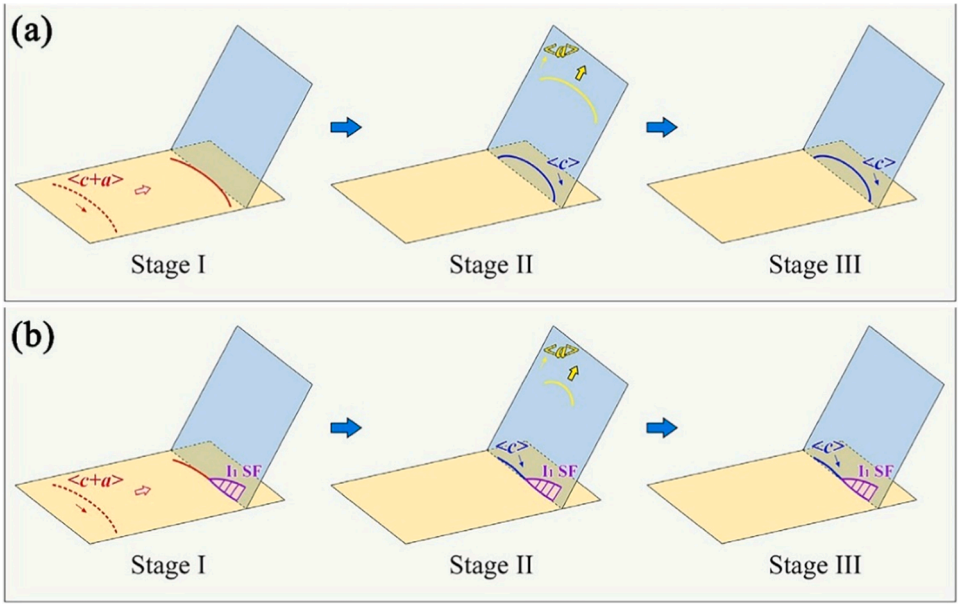

Fig. 20. Schematic diagram showing the <c + a> dislocation decomposition mechanisms [166]: (a) <c + a> dislocation completely dissociates into a sessile <c> dislocation and a glissile <a> dislocation in a cross-slip process; (b) segmental decomposition of a <c + a> dislocation. Reproduced with permission from Ref. [166].

<a> dislocation to Shockley partial pairs on a basal plane. Examples of I1 and I2 faults in a Mg-Y alloy are shown in Fig. 21 [176].

4.2. The schemes to improve plasticity

According to literature review, there are three effective ways to improve the tensile plasticity of Mg alloys at room temperature: (1) adjusting alloy compositions, (2) grain refinement, and (3) increasing the deformation temperature.

4.2.1. Adjusting the alloy composition to increase plasticity

The addition of alloying elements can alter the CRSS of various deformation modes, can thus potentially promote non-basal slip by reducing the difference of critical stress between basal and non-basal slip, thereby improving the ductility of Mg alloys at room temperature. Liu et al. [177] studied the electron work function (EWF) of 63 solutes, and proposed the principle for selecting appropriate solutes to improve the plasticity of Mg alloys. Their results revealed that adding solutes with the EWF lower than Mg can simultaneously improve the

Table 3
Independent twinning systems in HCP Mg alloys [167–171].

Type	Twin Plane	Twin Direction	Rotation angle
Primary twin	$\{10\bar{1}1\}$	$<10\bar{1}2>$	56°
	$\{10\bar{1}2\}$	$<10\bar{1}1>$	86°
	$\{10\bar{1}3\}$	$<30\bar{3}2>$	64°
	$\{11\bar{2}1\}$	$<11\bar{2}6>$	34°
Secondary twin	$\{10\bar{1}1\}-\{10\bar{1}2\}$	$<10\bar{1}2>-<10\bar{1}1>$	38°
	$\{10\bar{1}3\}-\{10\bar{1}2\}$	$<30\bar{3}2>-<10\bar{1}1>$	22°

Table 4
Types of SFs in HCP Mg alloys [175].

Type	Stacking order	Stacking fault energy ($mJ•m^{-2}$)
I1	•••ABAB**ABC**BCBCB•••	17.98
I2	•••ABAB**ABCA**CACA•••	33.84
E	•••ABAB**ABCAB**ABAB•••	52.57
T2	•••ABAB**ABCBA**BABA•••	40.55

strength and plasticity of the Mg alloy; adding solutes with higher EWF can improve the strength of the Mg alloy at the cost of plasticity, as shown in Fig. 22a. At room temperature, coarse-grained Mg has low strength and poor tensile plasticity. During plastic deformation of a coarse-grained Mg metal, high densities of basal <a> dislocations can easily form throughout deformed Mg grains [178], but in contrast the <c + a> dislocations tend to accumulate into band structures at isolated local areas, as shown in Fig. 22b [179].

Both first-principles calculations and experimental work show that the addition of RE alloying elements, such as Y, Gd, Er, Ho, etc., can promote activations of non-basal slip systems in Mg alloys, as shown in Fig. 22c [180]. Therefore, RE alloying is an effective method to strengthen and toughen Mg alloys [126,181–185].

Sandlöbes et al. [178] compared the tensile deformation mechanisms in Mg metal and Mg-Y alloy, and found that the active deformation modes in a Mg metal were mainly basal <a> slip and tensile twinning. In contrast, multiple twinning systems and pyramidal <c + a> dislocation slip are activated in the Mg-Y series alloys for significantly improved plasticity. The activations of prismatic and pyramidal slip systems in Mg alloys are attributed to Y alloying [186]. Moreover, Y alloying can promote cross-slip of <c + a> dislocation, benefitting both strength and ductility, as shown in Fig. 23 [35]. Appropriate addition of Al, Zn and Y elements can reduce the SF energy on pyramidal plane to be even lower than the basal plane; therefore, slip and cross-slip on pyramidal plane are promoted [187–189]. Ding et al. [180] used the xz-relax method to study the influence of the seven alloying elements (Y, Ca, Al, Tb, Dy, Ho, Er) on the generalized SF energy curves of the $\{11\bar{2}2\}<11\bar{2}3>$ slip system. The result presented in Fig. 22c shows that the width of potential-energy surface for Mg alloy is increased after alloying with Y, Ca, Tb, Dy, Ho and Er, except Al, indicating that adding these elements can reduce the global unstable SF energy for promoting the pyramidal <c + a> slip.

4.2.2. *Grain refinement for improved plasticity*

Grain refinement can significantly improve the strength, ductility and toughness of Mg alloys. Therefore, extensive research has been conducted in the last two decades to investigate grain refinement of Mg and Mg alloys to ultra-fine grain and nanocrystalline regimes. Reducing the grain sizes can inhibit twinning and promote non-basal slip. Sun et al. [190] found that the <c> dislocation density in a Mg alloy increased with the decrease of grain size in the submicron regime (0.1–1 μm), while the density of deformation twins decreased. In other words, the dominated deformation mechanism changed from twinning to

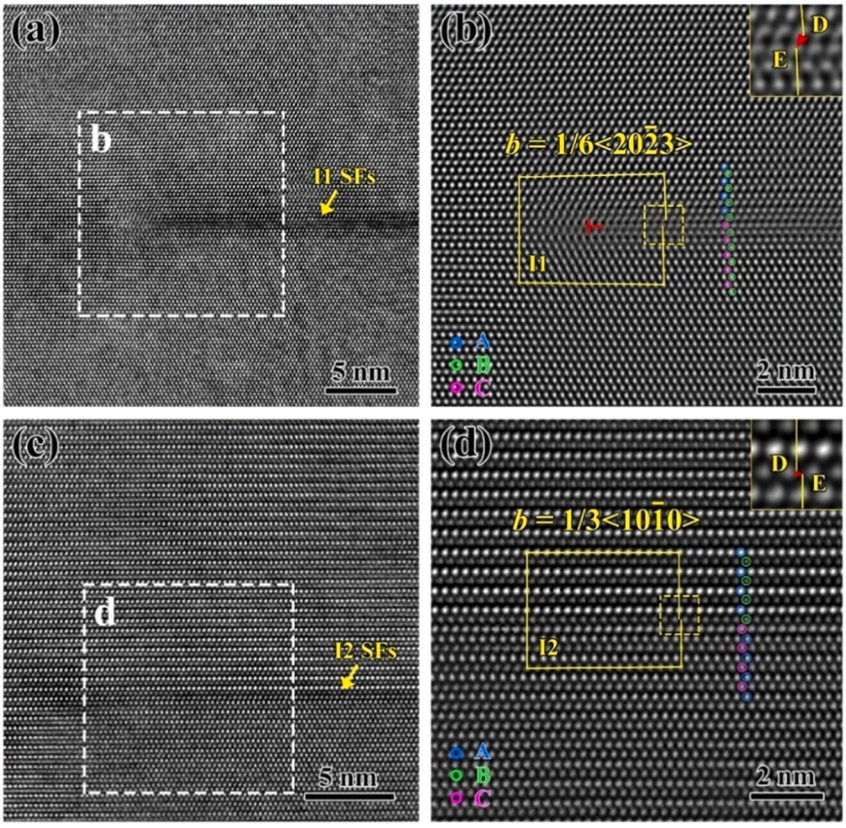

Fig. 21. High-resolution TEM images obtained at the $[2\bar{1}\bar{1}0]$ axis in a Mg-3Y alloy: (a) I1 faults; (b) a $1/6<20\bar{2}3>$ Frank partial; (c) I2 faults; (d) a $1/3<10\bar{1}0>$ Shockley partial. The insets show the Burgers vectors [176]. Reproduced with permission from Ref. [176].

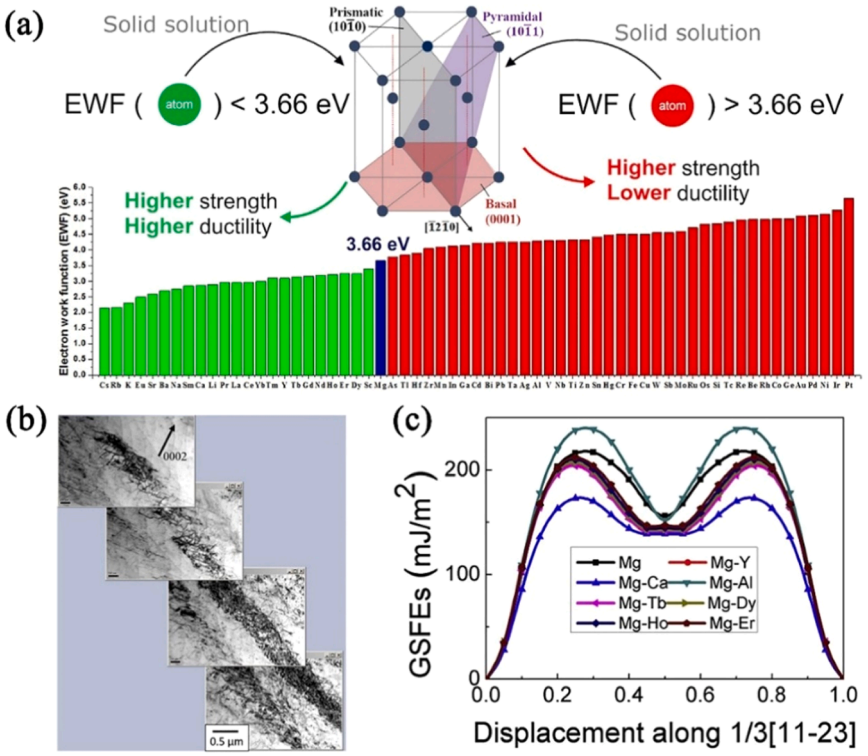

Fig. 22. (a) EWF of solute elements in Mg [177]. (b) A band structure formed via dislocation accumulation [179]. (c) Symmetric generalized stacking fault energy curves for Mg and Mg alloys [180]. Reproduced with permissions from Ref. [177,179,180].

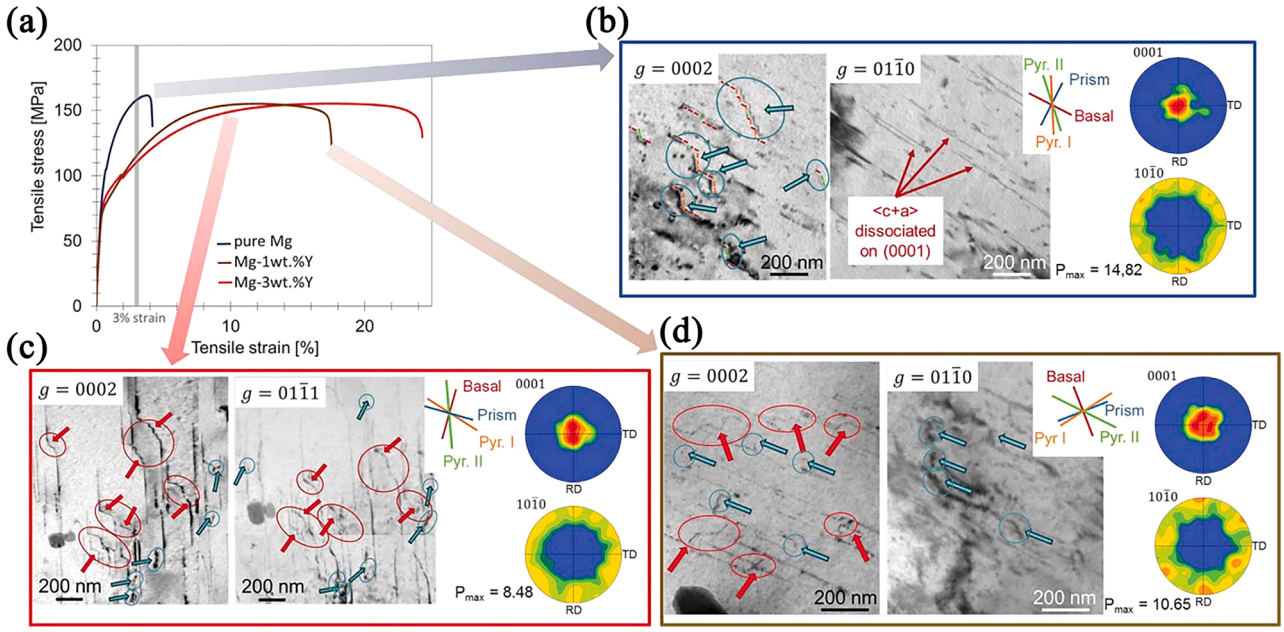

Fig. 23. (a) Tensile properties of Mg metal and Mg-Y alloys at room temperature; TEM and pole figures of deformed (b) Mg metal, (c) Mg-3 wt% Y and (d) Mg-1 wt% Y alloys [35]. Reproduced with permission from Ref. [35].

dislocation slip. Li et al. [191] reported that the compression deformation behavior of pure Mg at room temperature depends on the grain size. They found that sufficient reduction of grain size makes the twinning stress higher than the dislocation slip stress, thus changing the deformation mode from twinning to dislocation slip. Luo et al. [56] and Wei et al. [166] recently found that the strength and EF of Mg-3Gd alloy and pure Mg can be improved simultaneously by decreasing the grain sizes to a few micrometers, as shown in Fig. 24a-c. As shown in Figs. 24d-1 to d-3, a large number of <c + a> dislocations formed in fine grains with the sizes of a few micrometers. Usually, in TEM observation of Mg and Mg alloys, the two-beam conditions are set according to the invisibility criterion of $\mathbf{g} \bullet \mathbf{b} = 0$ to distinguish different types of dislocations, where **g** and **b** represent the reflection and Burgers vector, respectively. The invisibility criterion is shown in Table 5 [166,176]. For example,

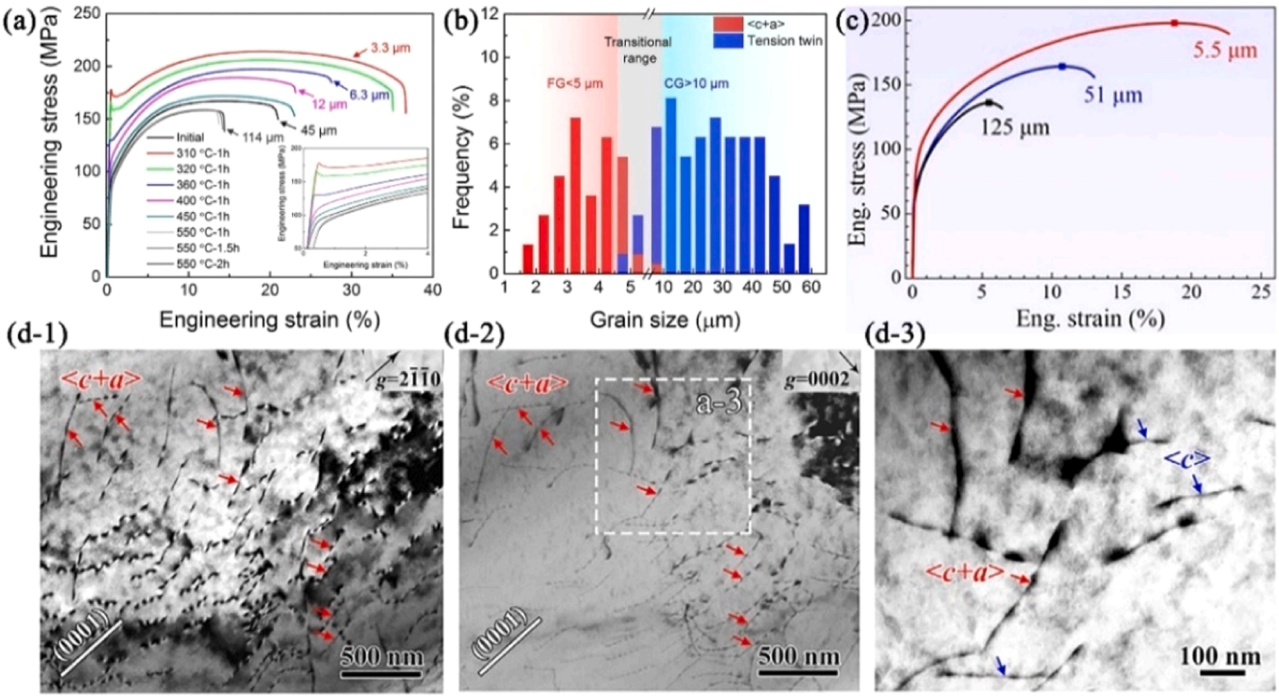

Fig. 24. (a, b) Tensile properties and the corresponding dominant deformation mechanisms of Mg-3Gd alloys with different grain sizes [56]; (c) Tensile properties of pure Mg with different grain sizes [166]; (d-1, d-2) TEM images showing <c + a> dislocations in a pure Mg with an average grain size of 5.5 μm; (d-3) An enlarged view of d-2 [166]. Reproduced with permissions from Ref. [56,166].

when the two-beam condition is set to $\mathbf{g} = 2\bar{1}\bar{1}0$, the <a> and <c + a> dislocations are both visible, while the <c> dislocation is invisible; when the two-beam condition is set to $\mathbf{g} = 0002$, the <c> and <c + a> dislocations are visible, but the <a> dislocation is invisible. Comparing Figs. 24d-1 and d-2, it can be seen that there is a large number of <c + a> dislocations in fine-grained Mg, indicating that grain refinement activates pyramidal slip systems and thus to improve the ductility significantly.

B. Figueiredo et al. [192] showed the high ductility of ultrafine grained pure Mg, and claimed that GB sliding plays a key role in low strain rate deformation of pure Mg with the grain sizes smaller than ~5 μm. Similarly, Zeng et al. [193,194] also showed high ductility of pure Mg with an average grain size of ~1 μm, and verified the dominant role of intergranular deformation in fine-grained Mg by in-situ scanning electron microscopy. They used in-situ TEM to show that dislocations easily slip to and annihilate at GBs in fine-grained Mg. In addition, Azghandi et al. [195] found that grain refinement can inhibit the growth of voids during failure of Mg alloys, and thus increase the EF of fine-grained Mg alloys.

In summary, grain refinement inhibits twinning in Mg and Mg alloys and facilitates activations of non-basal slip, during plastic deformation. As a result of grain refinement, the densities of GBs are significantly increased. Small grain size provides shortened intragranular mean free path for dislocation slip, and therefore reduces the chance for dislocation entanglement; the high density of GBs provides large numbers of boundary sources and sinks for dislocation slip. Moreover, ultrafine grains and nanograins are susceptible to GB sliding and grain rotation under high stress. Comprehensive coordination of the abovementioned grain size effects can delay the occurrence of local stress concentration and hence to improve the plasticity of Mg and Mg alloys. In short, significant grain refinement changes the deformation mechanisms, thereby significantly improves the plasticity of Mg and Mg alloys.

Table 5
Diffraction conditions and visibility of dislocations in Mg and Mg alloys [166,176].

Reflection vector, **g**	<a> dislocations (1/3< 11$\bar{2}$0 >) or Shockey partials (1/3< 10$\bar{1}$0 >)	<c> dislocations (<0001 >)	<c + a> dislocations (1/3< 11$\bar{2}$3 >) or Frank partials (1/6< 20$\bar{2}$3 >)
$\mathbf{g} = 2\bar{1}\bar{1}0$	√	×	√
$\mathbf{g} = 0\bar{1}10$	√	×	√
$\mathbf{g} = 0002$	×	√	√
$\mathbf{g} = 01\bar{1}1$	√	√	√
$\mathbf{g} = 0\bar{1}11$	√	√	√

4.2.3. *Increasing the deformation temperature to increase plasticity*

Temperature as an important source of thermal energy, poses significant effects on the deformation mechanisms and plasticity of Mg alloys. With the increase of deformation temperature, the number of activable slip systems increases, the strength decreases, and the plasticity improves significantly for Mg alloys. The CRSS for the pyramidal <c + a> slip at room temperature is about two orders of magnitude larger than that for the basal slip [196]; therefore, the pyramidal <c + a> slip is very difficult to activate at room temperature. When the deformation temperature is increased to 300°C, the atomic mobility is dramatically enhanced, and the activation energy for the non-basal slip in the Mg alloy will decrease significantly; Then, non-basal slip systems can be activated just as easy as the basal slip systems [197]. Moreover, high temperature facilitates stable deformation of Mg alloy to ultra-high strains under SPD. In order to gain deep understanding of the plastic deformation mechanisms in Mg alloys at high temperature, for the ultimate purpose of improving high temperature formability of Mg alloys, scholars have carried out extensive research work. Máthis et al. [197] used X-ray diffraction techniques to study the increasing fraction of <c + a> dislocations in pure Mg with the increasing deformation temperature. Chapuis et al. [198] found that tensile twinning and basal slip in a single crystal Mg are less dependent on temperature, while the CRSS for compressive twinning, prismatic slip, and pyramidal II <c + a> slip decreases significantly with increasing temperature. Sim et al. [199] reported that when the deformation temperature is sufficiently high, the

deformation mechanism in the single crystal Mg changes from twinning to non-basal slip. Similarly, Ventura et al. [200] found that when the temperature is less than 423 K, the plastic deformation of a single crystal Mg is dominated by twinning; As the temperature increases, the CRSS for non-basal slip gradually decreases; Eventually, when the temperature is higher than 423 K, the deformation mechanism changes from twinning to non-basal slip. These results are shown in Fig. 25 [199–204]. So far, the principle for activating non-basal slip systems by high temperature has been successfully applied to the production of Mg alloy sheets at industrial scale.

In summary, basal slip systems in Mg alloys are easily activated at room temperature, but are insufficient for homogenous plastic deformation. Twinning, non-basal slip and SFs play very important roles in ensuring the homogeneous plastic deformation and enhanced plasticity for Mg and Mg alloys. The proven effective methods for improving the tensile plasticity of Mg alloys are: (1) adjusting alloy compositions, (2) grain refinement, (3) increasing deformation temperature. To date, our knowledge about the grain size effect on deformation mechanisms in Mg and Mg alloys are limited to ultrafine grained regime, as grain refinement to nanocrystalline regime is still a challenge.

5. Strategies to improve the thermal stability of Mg alloys

Thermal stability refers to the ability of a material to withstand high temperature without significant change in microstructures and mechanical properties. The thermal stability of a material is crucial for the industrial applications, especially in the service environment concerning elevated temperature and high pressure. Unfortunately, Mg and Mg alloys usually have poor thermal stabilities [205]. Mg alloys are prone to dislocation recovery, grain growth and dissolution of secondary phase under high-temperature conditions, leading to decrease in strength. Currently, many of the research work regarding the thermal stability of Mg alloys primarily focus on improving the GB stability [206]. Moreover, some studies have indicated that the stability of precipitates also plays a significant role in determining the thermal stability of Mg alloys [207,208].

5.1. GB stability for enhanced thermal stability

The grain sizes of Mg alloys are very likely to increase in the high temperature environment, and the microstructures change accordingly, resulting in rapid decline in strength and catastrophic fracture. Controlling the thermal stability of the alloy lies fundamentally in controlling the stability of GBs [209]. The effective driving force P for grain growth and the growth velocity V can be expressed as follows [210]:

$$P = \gamma_{GB} K \tag{8}$$

$$V = MP = M\gamma_{GB} K \tag{9}$$

where M is the GB mobility, γ_{GB} is the GB energy, and K is the local mean curvature. For ultrafine and nanocrystalline Mg alloys, the GB curvature is large and the stored energy is high, therefore the driving force for grain growth is large. Apparently, the thermal stabilities of ultrafine and nanocrystalline Mg alloys are significantly lower than their coarse-grained counterparts. The grain growth behavior of ultrafine/nanocrystalline Mg alloys is not only affected by temperature and time, but also by the deformation history, alloying elements, impurity content, secondary phases, porosity and microscopic strain. According to literatures [211,212], the so far practical method for improving the thermal stability of Mg alloys is alloying.

Some solute atoms can significantly enhance the stability of GBs in two ways: (1) segregation of solute atoms to GBs to form interface complexions or precipitates, resulting in ordering of lattice structures at the GBs and hence reduce the GB energy and improve the GB stability [206,212]; (2) solute atoms at GBs poses pinning effect that lowers the mobility of the GBs, and thus improves the GB stability [10,206]. An interface complexion is an interface-stabilized state that has a structure and composition different from that of the matrix, and remain confined in a thickness of a few atomic layers. Interface complexions can form at SFs, twin boundaries and GBs in deformed Mg-RE alloys after heat treatment at medium temperatures [213,214]. Interface complexions are much larger than clusters and even larger than precipitates in terms of planar areas, but the thickness is only a few atomic layers; Therefore, it is also called linear complexions [215]. Nie et al. [216] conducted HAADF-STEM analysis to resolve the periodic segregation structures on the $\{10\bar{1}1\}$, $\{10\bar{1}2\}$ and $\{10\bar{1}3\}$ twin planes in Mg-Gd and Mg-Zn alloys at the atomic scale, as shown in Fig. 26. Xie et al. [173] studied the linear complexions at the $\{10\bar{1}1\}$ twin interfaces in a Mg-Nd alloy.

Zhou et al. [147] conducted systematic study on the interfacial segregation in Mg-Gd-Y alloys, and some results are shown in Fig. 27a. Segregations of Ag and Gd to different types of twin boundaries in the Mg-Gd-Y alloy are studied in detail. The thermodynamics and stability of the interfacial segregation structures were also studied. Xiao et al. conducted heat treatment to a Mg-Gd-Y alloy in the temperature range 250–400°C. As shown in Fig. 27b, both intragranular precipitates and linear complexions are seen in the Mg-Gd-Y alloy after annealing at 250°C. In contrast, after annealing treatment at 350°C, all of the

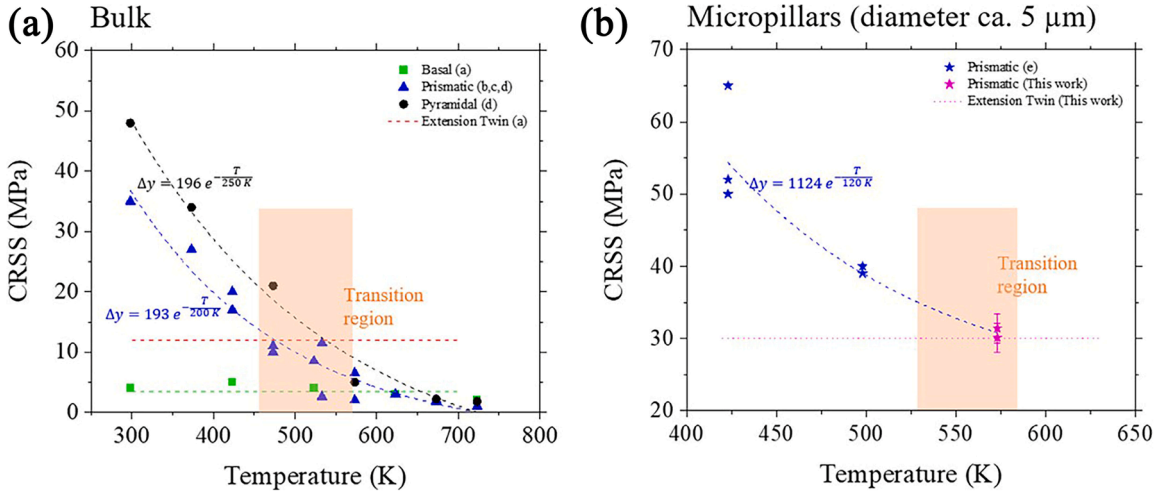

Fig. 25. CRSS versus temperature for basal and non-basal slip in pure Mg, under the condition $\dot{\varepsilon} = 10^{-3}$ s^{-1}: (a) Bulk samples; (b) Micropillars [199–204]. Reproduced with permission from Ref. [200].

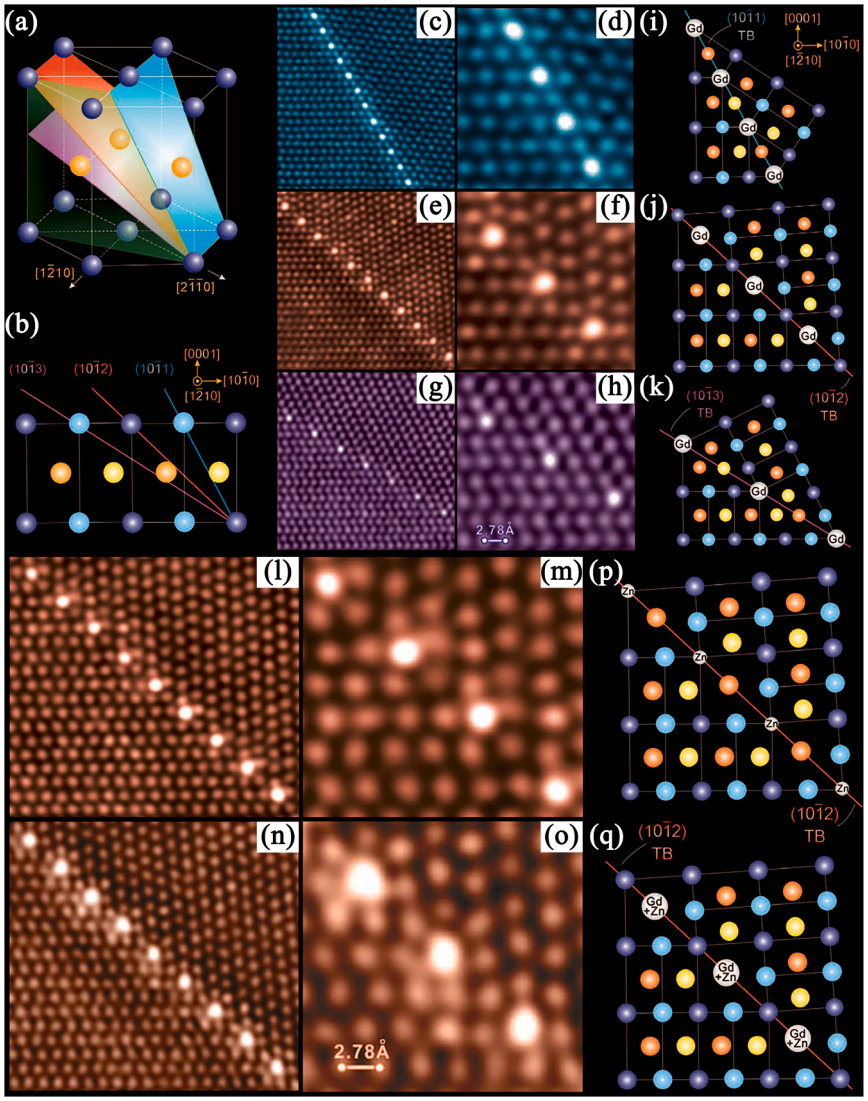

Fig. 26. (a) Schematic illustration and (b) [1$\bar{2}$10] projected view of α-Mg lattice; HAADF-STEM images showing (c, d) {10$\bar{1}$1}, (e, f) {10$\bar{1}$2}, and (g, h) {10$\bar{1}$3} twin boundaries in Mg-Gd alloys; (i-k) schematics showing atomic arrangements at the corresponding twin boundaries. HAADF-STEM images showing {10$\bar{1}$2} TBs in (l, m) Mg-1.9 at% Zn and (n, o) Mg-1.0 at% Gd-0.4 at% Zn-0.2 at% Zr alloys; (p, q) schematics showing atomic/elemental arrangements at the {10$\bar{1}$2} twin boundaries [216]. Reproduced with permission from Ref. [216].

intragranular precipitates disappeared, but the linear complexions remained. According to the work by Xiao et al., the linear complexions in the Mg-Gd-Y alloy is stable up to the annealing temperature of 400°C [217]. Tang et al. [112] found that the addition of Gd and Y elements to a Mg alloy facilitates nano-crystallization during SPD. Moreover, the SPD Mg-Gd-Y-Zr alloy with an average grain size of 80 nm, show thermal stability up to 250°C, due to the strong pinning effect of precipitates on GBs.

Fig. 28 [218] shows that solute segregation assisted nano-crystallization during annealing of a cold-rolled Mg-Ag alloy. During cold rolling, non-basal <c + a> dislocations entangled to form cell walls which were pinned by Ag segregation; upon heat treatment the Ag rich cell walls transformed into stable GBs. Moreover, due to the enrichment of Ag at the GBs, the nanocrystalline Mg-Ag alloy exhibits improved thermal stability at 150°C. Wu et al. [219] also conducted HAADF-STEM analysis to investigate the segregation structures at the {10$\bar{1}$1}, {10$\bar{1}$2} and {10$\bar{1}$3} twin boundaries in a Mg-Ag binary alloy. Substitutional segregation of Ag is observed at {10$\bar{1}$1} and {10$\bar{1}$2} twin boundaries, and a unique composite type segregation with two substitutional columns and one interstitial column in each periodic segregation unit is observed at the {10$\bar{1}$3} twin boundaries.

In addition, reinforcement particles in Mg matrix composites have similar microstructural stabilization effect to the precipitates in Mg alloys. The reinforcement particles can pose resistance against GB migration, inhibit grain growth, and thus significantly enhance the thermal stability of the composite. Su et al. [220] reported that the addition of Ti particles effectively suppressed grain growth. As a result, the nanocrystalline Ti/AZ61 Mg matrix composite exhibited superior thermal stability than the nanocrystalline AZ61 alloy in the temperature range of 573–723 K. In another study, Su et al. [221] demonstrated that adding submicron SiC particles effectively suppressed grain growth in the nanocrystalline AZ91 matrix, and therefore enhanced the thermal stability of the nanocrystalline SiC_P/AZ91 composite at 673 K. Zhang et al. [222] reported that the nanocrystalline AZ31–2.5 wt%V_P composite exhibited excellent thermal stability even at 450°C. They found that the V particles in the AZ31 matrix suppressed GB migration and increased the activation energy for grain growth, thereby effectively stabilized the microstructure at high temperatures. It is noted that the reinforcement particles shall be small in size, non-thermosensitive and uniformly dispersed for the purpose of thermal stability enhancement in

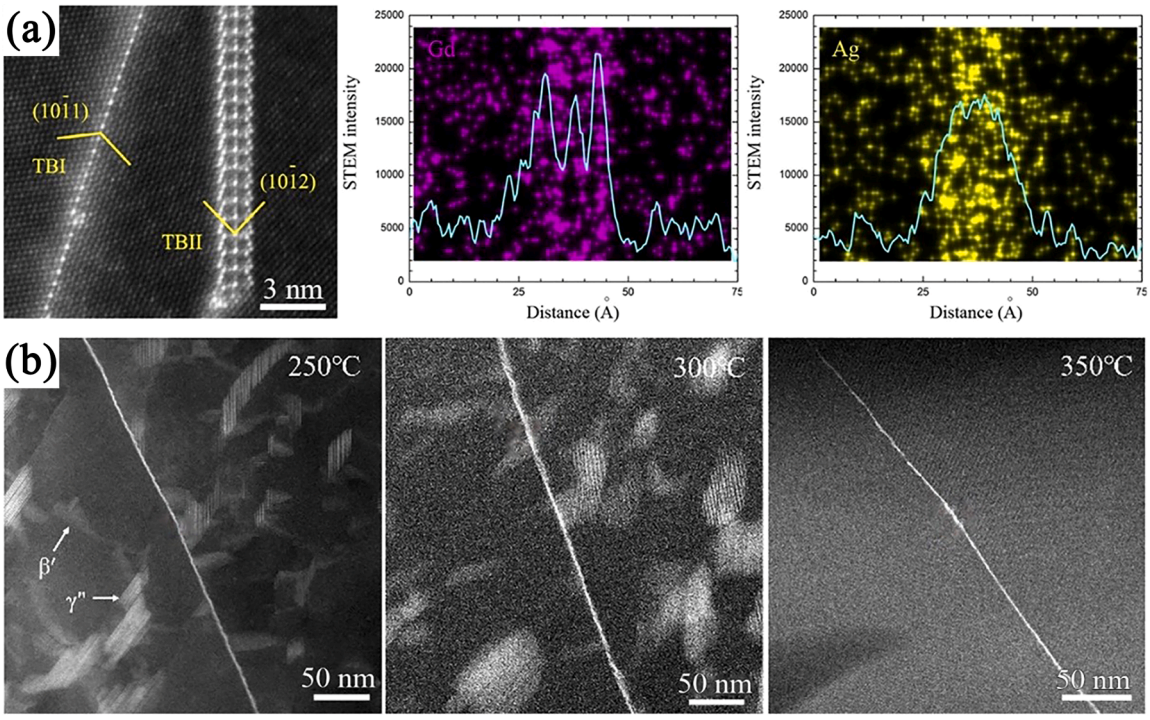

Fig. 27. Interfacial segregation structures in a Mg-Gd-Y-Ag alloy: (a) linear complexions formed at {10$\bar{1}$0} and {10$\bar{1}$2} twin boundaries, and elemental concentrations on a {10$\bar{1}$2} twin boundary; (b) thermal stabilities of intragranular precipitates and linear complexions at different annealing temperatures [147,217]. Reproduced with permissions from Ref. [147,217].

Mg matrix composites.

5.2. Precipitate stability for enhanced thermal stability

The thermal stability of precipitates directly affects the thermal stability of the bulk Mg alloys. Gerashi et al. [223] changed the content of Sr in the Mg-4Zn alloy, and annealed the samples at 400°C. The result shows that the grain size of the Mg-4Zn alloy without Sr increased significantly, while the grain size of the Sr-containing Mg-4Zn alloy was nearly unchanged after annealing. This is because the Mg_4Zn_7 particles in the Mg-4Zn alloy dissolve at 400°C, whereas the $Mg_{17}Sr_2$ particles are stable in the Sr-containing alloy. The study also demonstrates that when the Sr content exceeds 0.3 wt%, the precipitates coarsen, leading to decline of mechanical properties for the Mg-4Zn alloy; This is because coarse precipitates are likely to become crack initiation sites, leading to embrittlement of the alloy [11]. For another encouraging result, the Mg_2Sn phase in the Mg-Sn based alloys can remain stable even at 770°C, rendering the alloy with exceptionally high thermal stability and thus making them promising heat-resistant Mg alloys [207].

As mentioned in Section 3, precipitation strengthening plays a pivotal role in optimizing the mechanical properties of Mg alloys. The precipitation strengthening effect may persist in elevated temperatures. In high temperature environments, multiple dislocation slip systems are easily activated. While the easy activation of dislocation slip can enhance the plasticity of Mg alloys, it also leads to the reduction in strength. In high-temperature environments, precipitates can still hinder dislocation slip and climb, and thus can help sustain the strength and thermal stabilities of Mg alloys. Sun et al. [208] developed a Mg-4Sn-3Al-1Zn alloy by adding Sn to the AZ31 alloy, which exhibited excellent thermal stability at 230°C; in this work, the Mg_2Sn precipitates played a critical role in enhancing the high-temperature strength by hindering non-basal dislocation slip in the Mg-4Sn-3Al-1Zn alloy. Mg-Gd alloys usually exhibit excellent strength even at 250°C, primarily because the β' and γ'' phases can effectively hinder dislocation motion even under high-temperature conditions to provide the strengthening effect [224].

In summary, precipitates with high thermal stabilities play an essential role in enhancing the mechanical properties of Mg alloys at elevated temperatures.

6. Future perspectives

Mg alloys being so far the lightest metallic structural materials, are considered green engineering materials with the potential applications to fight back against environmental pollutions and energy crisis. However, the prerequisite for large scale applications of Mg alloys is to make the alloys sufficiently strong and ductile. Over the last 20 years, many researchers have made a lot of attempts to improve the mechanical properties of Mg alloys via grain refinement, alloying and changing processing conditions (strain rate and temperature). As a part of the attempts, a variety of Mg alloy forming processes have been adopted and developed: (1) the conventional metal forming processes including extrusion, rolling, forging, etc.; (2) SPD processes including ARB, CEC, ECAP, MDF, HPT, FSP, etc. Recently, new routes that employs RS for preparing bulk nanocrystalline Mg alloys, was investigated systematically. On the other hand, many rare-earth Mg alloys, rare-earth-free Mg alloys and Mg-based composites have been developed. The microstructural evolutions and deformation mechanisms of Mg alloys and composites under different deformation conditions have been studied systematically by means of experimental and simulation techniques, and a wealth of research results have been obtained. A large number of research results provides important guidance for the future development of high strength and high toughness Mg alloys.

In this review article, we make a bold prediction for the future development of Mg alloys:

1. With the development of nano-scale and micro-scale in-situ mechanical test methods and heat treatment methods, in-depth understanding of deformation mechanisms and heat induced microstructural evolutions in Mg alloys can be achieved.

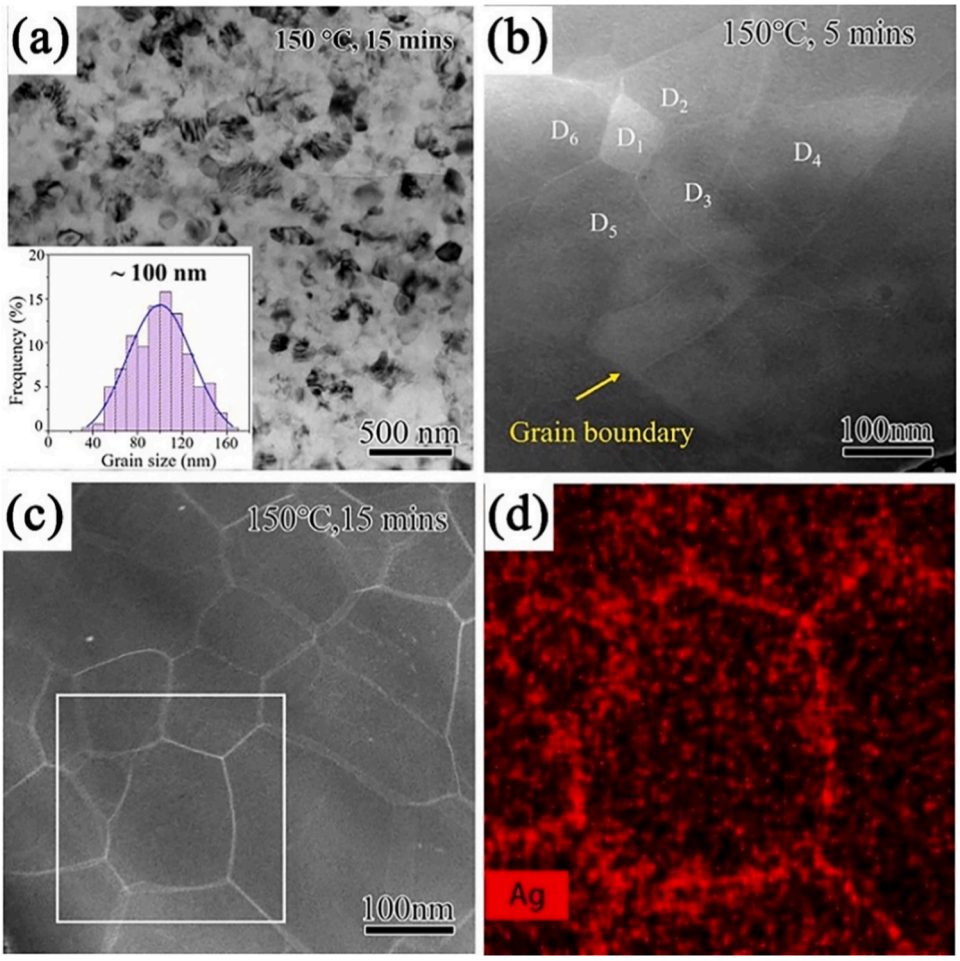

Fig. 28. (a) A TEM image showing the nanocrystalline structure in a Mg-Ag sample processed by cold rolling + annealing at 150°C for 15 mins (the inset is the grain size distribution histogram). HAADF images showing microstructures in the Mg-Ag alloy annealed at 150°C for (b) 5 mins and (c) 15 mins. (d) Energy-dispersive X-ray spectroscopy image of the area enclosed by the white rectangle in (c) [218]. Reproduced with permission from Ref. [218].

2. Development of multi-functional Mg alloys and Mg-based composites with combined properties including strength, ductility, toughness, corrosion resistance, thermal stability, damping capacity, electromagnetic shielding property, electrical conductivity and thermal conductivity, will keep going forward at an ever faster pace.
3. The development of advanced, low-cost, high-efficiency Mg alloy forming technologies will make it possible to prepare bulk nanocrystalline Mg alloys with engineering application values, and to realize the large-scale applications of Mg alloys.

CRediT authorship contribution statement

Cao Yang: Writing – review & editing, Funding acquisition. **Li Zhenghao:** Writing – original draft, Data curation, Conceptualization. **Xu Mengning:** Writing – original draft, Data curation. **zhao yonghao:** Writing – review & editing, Funding acquisition, Conceptualization.

Declaration of Competing Interest

The authors declare that they have no known competing financial interests or personal relationships that could have appeared to influence the work reported in this paper.

Acknowledgments

The authors would like to acknowledge financial supports from National Key R&D Program of China (Grant No. 2021YFA1200203), National Natural Science Foundation of China (Grant No. 51971112, 51225102, 52071181), Jiangsu Province Leading Edge Technology Basic Research Major Project (BK20222014). The authors also want to acknowledge the support from the Jiangsu Key Laboratory of Advanced Micro-Nano Materials and Technology, and the Center of Analytical Facilities of Nanjing University of Science and Technology.

Data availability

Data will be made available on request.

References

[1] J. Zhang, J. Miao, N. Balasubramani, D.H. Cho, T. Avey, C.Y. Chang, A.A. Luo, Magnesium research and applications: past, present and future, J. Magnes. Alloy 11 (2023) 3867–3895.
[2] J. Hou, D. Li, Z. Liu, Z. Ji, S. Guan, C. Li, X. Qiao, I.S. Golovin, M. Zheng, Structure-function integrated magnesium alloys and their composites, J. Magnes. Alloy 11 (2023) 3511–3544.
[3] M.J.A. Santos, W.O. Júnior, J.K.L. Ribeiro, N.C. Maciel, I.N. Bastos, J.N. Pereira, P.N. da Costa Souza, H.C. Pinto, E.P. da Silva, Zinc oxide coating impact on corrosion of ZK60 magnesium alloys in simulated body fluid, J. Alloy. Compd. 1002 (2024) 175339.
[4] B. Peng, H. Xu, F. Song, P. Wen, Y. Tian, Y. Zheng, Additive manufacturing of porous magnesium alloys for biodegradable orthopedic implants: process, design, and modification, J. Mater. Sci. Technol. 182 (2024) 79–110.
[5] J. She, J. Chen, X. Xiong, Y. Yang, X. Peng, D. Chen, F. Pan, Research advances of magnesium and magnesium alloys globally in 2023, J. Magnes. Alloy 12 (2024) 3441–3475.

[6] B. Liu, J. Yang, X. Zhang, Q. Yang, J. Zhang, X. Li, Development and application of magnesium alloy parts for automotive OEMs: a review, J. Magnes. Alloy 11 (2023) 15–47.

[7] J. Yang, Z. Zhu, S. Han, Y. Gu, Z. Zhu, H. Zhang, Evolution, limitations, advantages, and future challenges of magnesium alloys as materials for aerospace applications, J. Alloy. Compd. 1008 (2024) 176707.

[8] P. Peng, H. Xue, J. She, J. Zhang, A. Tang, S. Long, C. Zhang, Q. Yang, F. Pan, Ultrafine-grained Mg alloy: preparation, properties, design strategy, J. Mater. Res. Technol. 29 (2024) 4480–4504.

[9] D. Aksenov, A. Nazarov, M. Shishkunova, R. Asfandiyarov, A. Raab, Y. Sementeeva, Bulk ultrasonic treatment of magnesium and Mg-Zn-Zr alloy subjected to ECAP, J. Alloy. Compd. 1014 (2025) 178632.

[10] L. Xiao, P. Peng, S. Zhou, X. Wan, S. Long, C. Zhang, J. Zhang, C. Ran, J. Luo, J. She, F. Pan, Uncovering the synergistic role of trace Ca/Zn in weakening texture and elevating strength-ductility balance in dilute Mg-0.5Mn alloys, J. Alloy. Compd. 1010 (2025) 177629.

[11] Z. Zheng, Z. Dong, B. Jiang, Y. Cheng, A. Zhang, J. Song, T. Li, F. Pan, Evolution of strength with rare-earth content in highly-alloyed Mg-Gd-Y alloys, Scr. Mater. 238 (2024) 115772.

[12] S. Nandy, S.P. Tsai, L. Stephenson, D. Raabe, S. Zaefferer, The role of Ca, Al and Zn on room temperature ductility and grain boundary cohesion of magnesium, J. Magnes. Alloy 9 (2021) 1521–1536.

[13] Z. Wang, X. Zhao, S. Li, J. Yu, Strengthening mechanism based on dislocation-twin interaction under room temperature multi-directional forging of AZ80 Mg alloy, J. Mater. Res. Technol. 29 (2024) 3656–3672.

[14] X. Wang, W. Chen, Y. Yu, W. Wu, W. Wang, D. Fang, W. Zhang, J. Sun, Enhancing yield strength and quantifying relationship with microstructure in magnesium alloys through work hardening, J. Magnes. Alloy (2024) (In Press).

[15] L. He, J. Zheng, M. Xu, T. Li, D. Yin, B. Jiang, F. Pan, H. Zhou, Towards extraordinary strength-ductility synergy in pure Mg via dislocation transmutation, Int. J. Plast. 183 (2024) 104160.

[16] L. Gu, A. Meng, X. Chen, Y. Zhao, Simultaneously enhancing strength and ductility of HCP titanium via multi-modal grain induced extra <c + a> dislocation hardening, Acta Mater. 252 (2023) 118949.

[17] K. Edalati, A.Q. Ahmed, S. Akrami, K. Ameyama, V. Aptukov, R.N. Asfandiyarov, M. Ashida, V. Astanin, A. Bachmaier, V. Beloshenko, E.V. Bobruk, K. Bryła, J. M. Cabrera, A.P. Carvalho, N.Q. Chinh, I.C. Choi, R. Chulist, J.M. Cubero-Sesin, G. Davdian, M. Demirtas, S. Divinski, K. Durst, J. Dvorak, P. Edalati, S. Emura, N. A. Enikeev, G. Faraji, R.B. Figueiredo, R. Floriano, M. Fouladvind, D. Fruchart, M. Fuji, H. Fujiwara, M. Gajdics, D. Gheorghe, Ł. Gondek, J.E. González-Hernández, A. Gornakova, T. Grosdidier, J. Gubicza, D. Gunderov, L. He, O. F. Higuera, S. Hirosawa, A. Hohenwarter, Z. Horita, J. Horky, Y. Huang, J. Huot, Y. Ikoma, T. Ishihara, Y. Ivanisenko, J. Jang, A.M. Jorge Jr, M. Kawabata-Ota, M. Kawasaki, T. Khelfa, J. Kobayashi, L. Kommel, A. Korneva, P. Kral, N. Kudriashova, S. Kuramoto, T.G. Langdon, D.H. Lee, V.I. Levitas, C. Li, H.W. Li, Y. Li, Z. Li, H.J. Lin, K.D. Liss, Y. Liu, D.M.M. Cardona, K. Matsuda, A. Mazilkin, Y. Mine, H. Miyamoto, S.C. Moon, T. Müller, J.A. Muñoz, M.Y. Murashkin, M. Naeem, M. Novelli, D. Olasz, R. Pippan, V.V. Popov, E.N. Popova, G. Purcek, P. de Rango, O. Renk, D. Retraint, Á. Révész, V. Roche, P. Rodriguez-Calvillo, L. Romero-Resendiz, X. Sauvage, T. Sawaguchi, H. Sena, H. Shahmir, X. Shi, V. Sklenicka, W. Skrotzki, N. Skryabina, F. Staab, B. Straumal, Z. Sun, M. Szczerba, Y. Takizawa, Y. Tang, R.Z. Valiev, A. Vozniak, A. Voznyak, B. Wang, J.T. Wang, G. Wilde, F. Zhang, M. Zhang, P. Zhang, J. Zhou, X. Zhu, Y.T. Zhu, Severe plastic deformation for producing superfunctional ultrafine-grained and heterostructured materials: an interdisciplinary review, J. Alloy. Compd. 1002 (2024) 174667.

[18] X. Cui, W. Liu, Y. Yang, Y. Zhang, R. Li, G. Wei, Q. Li, B. Jiang, X. Peng, F. Pan, High-strength Mg-6Li-3Al-0.4Ce alloy fabricated by rotary swaging, Scr. Mater. 243 (2024) 115954.

[19] G. Zhou, Y. Yang, Y. Luo, Q. Li, Q. Luo, Y. Zhang, B. Jiang, X. Peng, F. Pan, Synergistic improvement of strength and plasticity of Mg-6Li-3Al-1Sn alloy by microstructure regulation via rotary swaging, Mater. Res. Lett. 11 (2023) 1031–1039.

[20] Z. Li, M. Xu, K. Zhou, Y. Cao, Y. Zhao, Preparing strong and ductile AZ80 Mg alloy via warm rotary swaging, J. Mater. Res. Technol. 34 (2025) 807–818.

[21] Y.Q. Li, F. Li, F.W. Kang, H.Q. Du, Z.Y. Chen, Recent research and advances in extrusion forming of magnesium alloys: a review, J. Alloy. Compd. 953 (2023) 170080.

[22] M. Ebrahimi, Q. Wang, S. Attarilar, A comprehensive review of magnesium-based alloys and composites processed by cyclic extrusion compression and the related techniques, Prog. Mater. Sci. 131 (2023) 101016.

[23] H. Wang, X.C. Luo, D.T. Zhang, C. Qiu, D.L. Chen, High-strength extruded magnesium alloys: a critical review, J. Mater. Sci. Technol. 199 (2024) 27–52.

[24] Y. Jiang, Q. Le, Y. Zhu, Q. Liao, T. Wang, L. Bao, P. Wang, Review on forming process of magnesium alloy characteristic forgings, J. Alloy. Compd. 970 (2024) 172666.

[25] L. Liu, Z.M. Zhang, Z.M. Yan, Y. Xue, Effect of annealing treatment on the homogeneity of microstructure and mechanical properties in Mg-Gd-Y-Zn-Zr rotary backward extruded tubular, J. Alloy. Compd. 978 (2024) 173463.

[26] M. Hashemi, R. Alizadeh, T.G. Langdon, Recent advances using equal-channel angular pressing to improve the properties of biodegradable Mg-Zn alloys, J. Magnes. Alloy 11 (2023) 2260–2284.

[27] P. Knochel, A flash of magnesium, Nat. Chem. 1 (2009) 740.

[28] W. Chen, W. Wu, W. Wang, W. Zhang, X. Liu, H.S. Kim, Adjusting approaches of basal texture for improvement of tension-compression asymmetry in extruded magnesium alloys, Mater. Res. Lett. 11 (2023) 563–570.

[29] T.M. Pollock, Weight loss with magnesium alloys, Science 328 (2010) 986–987.

[30] W. Xu, S. Ouyang, L. Deng, G. Zhu, X. Chen, F. Pan, Enhanced mechanical properties and electromagnetic interference shielding effectiveness in Mg-6Zn-1Y-1La-0.5Zr alloy sheet by hot deformation, J. Alloy. Compd. 1003 (2024) 175716.

[31] S. Tang, Z. Kou, T. Xin, Z. Zhang, T. Feng, T. Luo, S. Lan, G. Wilde, B. Jiang, Achieving high strength via solutes co-clustering and solvents redistribution in an ultralightweight BCC magnesium alloy, Mater. Res. Lett. 11 (2023) 556–562.

[32] Z. Wang, J. Song, Y. Peng, New insights and perspectives into biodegradable metals in cardiovascular stents: a mini review, J. Alloy. Compd. 1002 (2024) 175313.

[33] T. Wang, M. Zha, C. Du, H.L. Jia, C. Wang, K. Guan, Y. Gao, H.Y. Wang, High strength and high ductility achieved in a heterogeneous lamella-structured magnesium alloy, Mater. Res. Lett. 11 (2022) 187–195.

[34] Z. Wu, W.A. Curtin, The origins of high hardening and low ductility in magnesium, Nature 526 (2015) 62–67.

[35] Z. Wu, R. Ahmad, B. Yin, S. Sandlöbes, W.A. Curtin, Mechanistic origin and prediction of enhanced ductility in magnesium alloys, Science 359 (2018) 447–452.

[36] C. Yan, Y. Xin, X.B. Chen, D. Xu, P.K. Chu, C. Liu, B. Guan, X. Huang, Q. Liu, Evading strength-corrosion tradeoff in Mg alloys via dense ultrafine twins, Nat. Commun. 12 (2021) 4616.

[37] G. Shen, S. Lyu, Q. Yu, X. Wang, M. Chen, Investigating the mechanical properties and corrosion resistance of extruded Mg-1Zn-xCaO (x=0, 0.5, 1.0 wt%) materials, J. Alloy. Compd. 1010 (2025) 177174.

[38] G. Wu, K.C. Chan, L. Zhu, L. Sun, J. Lu, Dual-phase nanostructuring as a route to high-strength magnesium alloys, Nature 545 (2017) 80–83.

[39] L.Y. Chen, J.Q. Xu, H. Choi, M. Pozuelo, X. Ma, S. Bhowmick, J.M. Yang, S. Mathaudhu, X.C. Li, Processing and properties of magnesium containing a dense uniform dispersion of nanoparticles, Nature 528 (2015) 539–543.

[40] T. Xin, Y. Zhao, R. Mahjoub, J. Jiang, A. Yadav, K. Nomoto, R. Niu, S. Tang, F. Ji, Z. Quadir, D. Miskovic, J. Daniels, W. Xu, X. Liao, L.Q. Chen, K. Hagihara, X. Li, S. Ringer, M. Ferry, Ultrahigh specific strength in a magnesium alloy strengthened by spinodal decomposition, Science 7 (2021) 1–9.

[41] J.M. Song, T.X. Wen, J.Y. Wang, Vibration fracture properties of a lightweight Mg-Li-Zn alloy, Scr. Mater. 56 (2007) 529–532.

[42] G. Tian, J. Wang, S. Wang, C. Xue, X. Yang, H. Su, Z. Yang, C. Yan, X. Liu, R. Dou, Achieving ultra-high stiffness by solidifying and precipitating micro-compounds in HCP/BCC dual matrix of a new Mg-Li alloy, J. Alloy. Compd. 964 (2023) 171324.

[43] R.Z. Valiev, Nanostructural design of superstrong metallic materials by severe plastic deformation processing, Microstructures 3 (2023) 2023004.

[44] D. Xu, M. Wang, T. Li, X. Wei, Y. Lu, A critical review of the mechanical properties of CoCrNi-based medium-entropy alloys, Microstructures 2 (2022) 2022001.

[45] Q. Shi, A.R. Natarajan, A. Van der Ven, J. Allison, Partitioning of Ca to metastable precipitates in a Mg-rare earth alloy, Mater. Res. Lett. 11 (2022) 222–230.

[46] R.G. Li, Y. Yan, H.C. Pan, H. Zhang, J.R. Li, G.W. Qin, B.S. Liu, Achieving a high-strength binary Mg-15Gd alloy by nano substructure with Gd segregation and nano clusters[1], Mater. Res. Lett. 10 (2022) 682–689.

[47] W. Fu, P. Dang, S. Guo, Z. Ren, D. Fang, X. Ding, J. Sun, Heterogeneous fiberous structured Mg-Zn-Zr alloy with superior strength-ductility synergy, J. Mater. Sci. Technol. 134 (2023) 67–80.

[48] Q.X. Ma, H.J. Yang, Z. Wang, X.H. Shi, P.K. Liaw, J.W. Qiao, High strength and ductility in partially recrystallized $Fe_{40}Mn_{20}Cr_{20}Ni_{20}$ high-entropy alloys at cryogenic temperature, Microstructures 2 (2022) 2022015.

[49] Y. Wan, B. Tang, Y. Gao, L. Tang, G. Sha, B. Zhang, N. Liang, C. Liu, S. Jiang, Z. Chen, X. Guo, Y. Zhao, Bulk nanocrystalline high-strength magnesium alloys prepared via rotary swaging, Acta Mater. 200 (2020) 274–286.

[50] K. Edalati, A. Bachmaier, V.A. Beloshenko, Y. Beygelzimer, V.D. Blank, W. J. Botta, K. Bryła, J. Čížek, S. Divinski, N.A. Enikeev, Y. Estrin, G. Faraji, R. B. Figueiredo, M. Fuji, T. Furuta, T. Grosdidier, J. Gubicza, A. Hohenwarter, Z. Horita, J. Huot, Y. Ikoma, M. Janeček, M. Kawasaki, P. Král, S. Kuramoto, T. G. Langdon, D.R. Leiva, V.I. Levitas, A. Mazilkin, M. Mito, H. Miyamoto, T. Nishizaki, R. Pippan, V.V. Popov, E.N. Popova, G. Purcek, O. Renk, Á. Révész, X. Sauvage, V. Sklenicka, W. Skrotzki, B.B. Straumal, S. Suwas, L.S. Toth, N. Tsuji, R.Z. Valiev, G. Wilde, M.J. Zehetbauer, X. Zhu, Nanomaterials by severe plastic deformation: review of historical developments and recent advances, Mater. Res. Lett. 10 (2022) 163–256.

[51] T. Wang, H. Zheng, R. Wu, J. Yang, X. Ma, M. Zhang, Preparation of fine-grained and high-strength Mg-8Li-3Al-1Zn alloy by accumulative roll bonding, Adv. Eng. Mater. 18 (2016) 304–311.

[52] L. Hou, T. Wang, R. Wu, J. Zhang, M. Zhang, A. Dong, B. Sun, S. Betsofen, B. Krit, Microstructure and mechanical properties of Mg-5Li-1Al sheets prepared by accumulative roll bonding, J. Mater. Sci. Technol. 34 (2018) 317–323.

[53] X. Rao, Y. Wu, X. Pei, Y. Jing, L. Luo, Y. Liu, J. Lu, Influence of rolling temperature on microstructural evolution and mechanical behavior of AZ31 alloy with accumulative roll bonding, Mater. Sci. Eng. A 754 (2019) 112–120.

[54] X. Luo, Z. Feng, T. Yu, T. Huang, R. Li, G. Wu, N. Hansen, X. Huang, Microstructural evolution in Mg-3Gd during accumulative roll-bonding, Mater. Sci. Eng. A 772 (2020) 138763.

[55] X. Luo, Z. Feng, R. Fu, T. Huang, G. Wu, X. Huang, The synergy of boundary engineering and segregation strategy towards high strength and ductility Mg-3Gd alloy, J. Alloy. Compd. 819 (2020) 153051.

[56] X. Luo, Z. Feng, T. Yu, J. Luo, T. Huang, G. Wu, N. Hansen, X. Huang, Transitions in mechanical behavior and in deformation mechanisms enhance the strength and ductility of Mg-3Gd, Acta Mater. 183 (2020) 398–407.
[57] Y. Tian, H. Huang, G. Yuan, W. Ding, Microstructure evolution and mechanical properties of quasicrystal-reinforced Mg-Zn-Gd alloy processed by cyclic extrusion and compression, J. Alloy. Compd. 626 (2015) 42–48.
[58] Q. Wang, Y. Mu, J. Lin, L. Zhang, H.J. Roven, Strengthening and toughening mechanisms of an ultrafine grained Mg-Gd-Y-Zr alloy processed by cyclic extrusion and compression, Mater. Sci. Eng. A 699 (2017) 26–30.
[59] E.E. Klu, D. Song, C. Li, G. Wang, B. Gao, A. Ma, J. Jiang, Achieving ultra-fine grains and high strength of Mg-9Li alloy via room-temperature ECAP and post rolling, Mater. Sci. Eng. A 833 (2022) 142371.
[60] X. Liu, L. Bian, F. Tian, S. Han, T. Wang, W. Liang, Microstructural evolution and mechanical response of duplex Mg-Li alloy containing particles during ECAP processing, Mater. Charact. 188 (2022) 111910.
[61] L. Bian, X. Liu, T. Wang, W. Liang, Y. Zheng, Influence of various initial microstructures on microstructure and mechanical property of ECAP processed Mg-8.4Li-3.58Al-0.36Si-0.05Ti-0.01B alloys, Mater. Sci. Eng. A 872 (2023) 144022.
[62] J. Suh, J. Victoria-Hernández, D. Letzig, R. Golle, W. Volk, Effect of processing route on texture and cold formability of AZ31 Mg alloy sheets processed by ECAP, Mater. Sci. Eng. A 669 (2016) 159–170.
[63] C. Wang, A. Ma, J. Sun, H. Liu, H. Huang, Z. Yang, J. Jiang, Effect of ECAP process on as-cast and as-homogenized Mg-Al-Ca-Mn alloys with different Mg_2Ca morphologies, J. Alloy. Compd. 793 (2019) 259–270.
[64] H. Huang, H. Liu, C. Wang, J. Sun, J. Bai, F. Xue, J. Jiang, A. Ma, Potential of multi-pass ECAP on improving the mechanical properties of a high-calcium-content Mg-Al-Ca-Mn alloy, J. Magnes. Alloy 7 (2019) 617–627.
[65] H. Liu, C. Sun, C. Wang, Y. Li, J. Bai, F. Xue, A. Ma, J. Jiang, Improving toughness of a Mg_2Ca-containing Mg-Al-Ca-Mn alloy via refinement and uniform dispersion of Mg_2Ca particles, J. Mater. Sci. Technol. 59 (2020) 61–71.
[66] Z. Yang, A. Ma, B. Xu, J. Jiang, H. Wu, J. Sun, Tailoring the microstructure and texture to achieve high strength in a high-Al content Mg alloy by stepless-temperature-reduction ECAP, Mater. Sci. Eng. A 841 (2022) 143023.
[67] C. Sun, H. Liu, C. Wang, J. Ju, G. Wang, J. Jiang, A. Ma, J. Bai, F. Xue, Y. Xin, Anisotropy investigation of an ECAP-processed Mg-Al-Ca-Mn alloy with synergistically enhanced mechanical properties and corrosion resistance, J. Alloy. Compd. 911 (2022) 165046.
[68] K. Bryła, M. Krystian, J. Horky, B. Mingler, K. Mroczka, P. Kurtyka, L. Lityńska-Dobrzyńska, Improvement of strength and ductility of an EZ magnesium alloy by applying two different ECAP concepts to processable initial states, Mater. Sci. Eng. A 737 (2018) 318–327.
[69] K.N. Li, Y.B. Zhang, Q. Zeng, G.H. Huang, B. Ji, D.D. Yin, Effects of semisolid treatment and ECAP on the microstructure and mechanical properties of Mg-6.52Zn-0.95Y alloy with icosahedral phase, Mater. Sci. Eng. A 751 (2019) 283–291.
[70] K. Bryła, Microstructure and mechanical characterisation of ECAP-ed ZE41A alloy, Mater. Sci. Eng. A 772 (2020) 138750.
[71] J. Horky, K. Bryła, M. Krystian, G. Mozdzen, B. Mingler, L. Sajti, Improving mechanical properties of lean Mg-Zn-Ca alloy for absorbable implants via double equal channel angular pressing (D-ECAP), Mater. Sci. Eng. A 826 (2021) 142002.
[72] L.B. Tong, J.H. Chu, W.T. Sun, Z.H. Jiang, D.N. Zou, S.F. Liu, S. Kamado, M. Y. Zheng, Development of a high-strength Mg alloy with superior ductility through a unique texture modification from equal channel angular pressing, J. Magnes. Alloy 9 (2021) 1007–1018.
[73] M. Gao, K. Yang, L. Tan, Z. Ma, Role of bimodal-grained structure with random texture on mechanical and corrosion properties of a Mg-Zn-Nd alloy, J. Magnes. Alloy 10 (2022) 2147–2157.
[74] J. Zhang, W. Zhang, L. Bian, W. Cheng, X. Niu, C. Xu, S. Wu, Study of Mg-Gd-Zn-Zr alloys with long period stacking ordered structures, Mater. Sci. Eng. A 585 (2013) 268–276.
[75] J. Zhang, Z. Kang, L. Zhou, Microstructure evolution and mechanical properties of Mg-Gd-Nd-Zn-Zr alloy processed by equal channel angular pressing, Mater. Sci. Eng. A 647 (2015) 184–190.
[76] M. Bleckmann, M. Eichhorst, M. Schuch, W. Kreuzer, V.H. Hammond, C. Spiller, L.W. Meyer, N. Herzig, The influence of selected ECAP-processing routes on the material properties of magnesium elektron 675, Mater. Sci. Eng. A 660 (2016) 108–117.
[77] W. Yang, G.F. Quan, B. Ji, Y.F. Wan, H. Zhou, J. Zheng, D.D. Yin, Effect of Y content and equal channel angular pressing on the microstructure, texture and mechanical property of extruded Mg-Y alloys, J. Magnes. Alloy 10 (2022) 195–208.
[78] Z. Gui, F. Wang, J. Zhang, D. Chen, Z. Kang, Precipitation behaviors and mechanical properties of a solution-treated Mg-Gd-Nd-Zn-Zr alloy during equal-channel angular pressing process, J. Magnes. Alloy 10 (2022) 239–248.
[79] F. Cao, J. Zhang, X. Ding, G. Xue, S. Liu, C. Sun, R. Su, X. Teng, Mechanical properties and microstructural evolution in a superlight Mg-6.4Li-3.6Zn-0.37Al-0.36Y alloy processed by multidirectional forging and rolling, Mater. Sci. Eng. A 760 (2019) 377–393.
[80] H. Huang, J. Zhang, Microstructure and mechanical properties of AZ31 magnesium alloy processed by multi-directional forging at different temperatures, Mater. Sci. Eng. A 674 (2016) 52–58.
[81] Z. Zhang, L. Yuan, M. Zheng, Q. Wei, D. Shan, B. Guo, Achievement of high strength and good ductility in the large-size AZ80 Mg alloy using a designed multi-directional forging process and aging treatment, J. Mater. Process. Technol. 311 (2023) 117828.
[82] S.H. Lu, D. Wu, R.S. Chen, E.H. Han, Reasonable utilization of {10-12} twin for optimizing microstructure and improving mechanical property in a Mg-Gd-Y alloy, Mater. Des. 191 (2020) 108600.
[83] L.B. Tong, J.H. Chu, W.T. Sun, C. Xu, D.N. Zou, K.S. Wang, S. Kamado, M. Y. Zheng, Achieving an ultra-high strength and moderate ductility in Mg-Gd-Y-Zn-Zr alloy via a decreased-temperature multi-directional forging, Mater. Charact. 171 (2021) 110804.
[84] C. Huang, C. Liu, S. Jiang, Y. Wan, Y. Gao, Inhomogeneous microstructure and mechanical anisotropy of multi-directional forged Mg-Gd-Y-Zn-Ag-Zr alloy, Mater. Sci. Eng. A 807 (2021) 140853.
[85] N. Ding, W. Du, X. Zhu, L. Dou, Y. Wang, X. Li, K. Liu, S. Li, Roles of LPSO phases on dynamic recrystallization of high strain rate multi-directional free forged Mg-Gd-Er-Zn-Zr alloy and its strengthening mechanisms, Mater. Sci. Eng. A 864 (2023) 144590.
[86] R. Zheng, T. Bhattacharjee, A. Shibata, T. Sasaki, K. Hono, M. Joshi, N. Tsuji, Simultaneously enhanced strength and ductility of Mg-Zn-Zr-Ca alloy with fully recrystallized ultrafine grained structures, Scr. Mater. 131 (2017) 1–5.
[87] S.V. Dobatkin, L.L. Rokhlin, E.A. Lukyanova, M.Y. Murashkin, T.V. Dobatkina, N. Y. Tabachkova, Structure and mechanical properties of the Mg-Y-Gd-Zr alloy after high pressure torsion, Mater. Sci. Eng. A 667 (2016) 217–223.
[88] Q.Y. Che, K.S. Wang, W. Wang, L.Y. Huang, T.Q. Li, X.P. Xi, P. Peng, K. Qiao, Microstructure and mechanical properties of magnesium-lithium alloy prepared by friction stir processing, Rare Met 40 (2021) 2552–2559.
[89] Y. Li, Y. Guan, Y. Liu, J. Zhai, K. Hu, J. Lin, Microstructure and tensile properties of the friction stir processed LA103Z alloy, Mater. Charact. 196 (2023) 112616.
[90] S.S. Nene, S. Zellner, B. Mondal, M. Komarasamy, R.S. Mishra, R.E. Brennan, K. C. Cho, Friction stir processing of newly-designed Mg-5Al-3.5Ca-1Mn (AXM541) alloy: microstructure evolution and mechanical properties, Mater. Sci. Eng. A 729 (2018) 294–299.
[91] H.J. Sharahi, M. Pouranvari, M. Movahedi, Strengthening and ductilization mechanisms of friction stir processed cast Mg-Al-Zn alloy, Mater. Sci. Eng. A 781 (2020) 139249.
[92] M. Vargas, S. Lathabai, P.J. Uggowitzer, Y. Qi, D. Orlov, Y. Estrin, Microstructure, crystallographic texture and mechanical behaviour of friction stir processed Mg-Zn-Ca-Zr alloy ZKX50, Mater. Sci. Eng. A 685 (2017) 253–264.
[93] Y. Huang, Y. Wang, X. Meng, L. Wan, J. Cao, L. Zhou, J. Feng, Dynamic recrystallization and mechanical properties of friction stir processed Mg-Zn-Y-Zr alloys, J. Mater. Process. Technol. 249 (2017) 331–338.
[94] J. Li, Y. Huang, F. Wang, X. Meng, L. Wan, Z. Dong, Enhanced strength and ductility of friction-stir-processed Mg-6Zn alloys via Y and Zr co-alloying, Mater. Sci. Eng. A 773 (2020) 138877.
[95] U. Rokkala, S. Bontha, M.R. Ramesh, V.K. Balla, Influence of friction stir processing on microstructure, mechanical properties and corrosion behaviour of Mg-Zn-Dy alloy, J. Mater. Sci. 58 (2023) 2893–2914.
[96] F.C. Liu, Z.Y. Ma, M.J. Tan, Facilitating basal slip to increase deformation ability in Mg-Mn-Ce Alloy by textural reconstruction using friction stir processing, Met. Mater. Trans. A 44 (2013) 3947–3960.
[97] G. Cao, D. Zhang, X. Luo, W. Zhang, W. Zhang, Effect of aging treatment on mechanical properties and fracture behavior of friction stir processed Mg-Y-Nd, Alloy, J. Mater. Sci. 51 (2016) 7571–7584.
[98] J. Han, J. Chen, L. Peng, S. Tan, Y. Wu, F. Zheng, H. Yi, Microstructure, texture and mechanical properties of friction stir processed Mg-14Gd alloys, Mater. Des. 130 (2017) 90–102.
[99] A.M. Jamili, A. Zarei-Hanzaki, H.R. Abedi, P. Minárik, R. Soltani, The microstructure, texture, and room temperature mechanical properties of friction stir processed Mg-Y-Nd alloy, Mater. Sci. Eng. A 690 (2017) 244–253.
[100] W. Zhang, L. Tan, D. Ni, J. Chen, Y.C. Zhao, L. Liu, C. Shuai, K. Yang, A. Atrens, M.C. Zhao, Effect of grain refinement and crystallographic texture produced by friction stir processing on the biodegradation behavior of a Mg-Nd-Zn alloy, J. Mater. Sci. Technol. 35 (2019) 777–783.
[101] B. Li, X. Hou, B. Teng, Effects of friction stir process and subsequent aging treatment on the microstructure evolution and mechanical properties of Mg-Gd-Y-Zn-Zr alloy, Mater. Charact. 155 (2019) 109832.
[102] Q. Deng, Y. Wu, N. Su, Z. Chang, J. Chen, L. Peng, W. Ding, Influence of friction stir processing and aging heat treatment on microstructure and mechanical properties of selective laser melted Mg-Gd-Zr alloy, Addit. Manuf. 44 (2021) 102036.
[103] J. Chen, Z. Li, J. Han, L. Peng, H. Fujii, Y. Wu, H. Cheng, Investigation on microstructure evolution of Mg-Gd-Zn-Zr alloys during friction stir processing by liquid CO_2 cooling assisted stop action, Mater. Sci. Eng. A 876 (2023) 145140.
[104] Y. Yang, X. Chen, J. Nie, K. Wei, Q. Mao, F. Lu, Y. Zhao, Achieving ultra-strong magnesium-lithium alloys by low-strain rotary swaging, Mater. Res. Lett. 9 (2021) 255–262.
[105] X. Chen, C. Liu, Y. Wan, S. Jiang, Z. Chen, Y. Zhao, Grain refinement mechanisms in gradient nanostructured AZ31B Mg alloy prepared via rotary swaging, Met. Mater. Trans. A 52 (2021) 4053–4065.
[106] X. Chen, C. Liu, S. Jiang, Z. Chen, Y. Wan, Effect of yttrium on nanocrystallization of magnesium alloys during cold rotary swaging, Mater. Charact. 184 (2022) 111696.
[107] J. Zou, L. Ma, W. Jia, Q. Le, G. Qin, Y. Yuan, Microstructural and mechanical response of ZK60 magnesium alloy subjected to radial forging, J. Mater. Sci. Technol. 83 (2021) 228–238.
[108] H. Chen, Y. Yang, F. Hu, X. Liu, F. Kong, X. Cui, W. Xie, G. Wei, Y. Yang, X. Peng, Y. Huang, Improvement of severe plastic deformation realized by several passes rotary swaging in the microstructure and properties of Mg-0.6Mn-0.5Al-0.5Zn-0.4Ca alloy, Mater. Sci. Eng. A 865 (2023) 144629.

[109] X. Chen, C. Liu, M. Fang, S. Jiang, Z. Chen, Y. Wan, Strengthening the Mg-Y-Zn alloy through the formation of nanoscale lamellar structures and nanograins, J. Alloy. Compd. 886 (2021) 161148.
[110] Z. Huang, C. Liu, S. Jiang, H. Xiao, X. Chen, Y. Wan, G. Zeng, Achieving high-strength nanocrystalline WE43 Mg alloy by a combination of cold rotary swaging and aging treatment, Vacuum 197 (2022) 110840.
[111] L. Tang, Y. Zhao, R.K. Islamgaliev, C.Y.A. Tsao, R.Z. Valiev, E.J. Lavernia, Y. T. Zhu, Enhanced strength and ductility of AZ80 Mg alloys by spray forming and ECAP, Mater. Sci. Eng. A 670 (2016) 280–291.
[112] L. Tang, Y. Zhao, R.K. Islamgaliev, R.Z. Valiev, Y.T. Zhu, Microstructure and thermal stability of nanocrystalline Mg-Gd-Y-Zr alloy processed by high pressure torsion, J. Alloy. Compd. 721 (2017) 577–585.
[113] H.Q. Sun, Y.N. Shi, M.X. Zhang, K. Lu, Plastic strain-induced grain refinement in the nanometer scale in a Mg alloy, Acta Mater. 55 (2007) 975–982.
[114] Q. Mao, Y. Zhang, J. Liu, Y. Zhao, Breaking material property trade-offs via macrodesign of microstructure, Nano Lett. 21 (2021) 3191–3197.
[115] W. Feng, Z. Wang, Q. Sun, Y. He, Y. Sun, Effect of thermomechanical processing via rotary swaging on grain boundary character distribution and intergranular corrosion in 304 austenitic stainless steel, J. Mater. Res. Technol. 19 (2022) 2470–2482.
[116] W.M. Gan, Y.D. Huang, R. Wang, Z.Y. Zhong, N. Hort, K.U. Kainer, N. Schell, H. G. Brokmeier, A. Schreyer, Bulk and local textures of pure magnesium processed by rotary swaging, J. Magnes. Alloy 1 (2013) 341–345.
[117] X. Chen, C. Liu, Y. Wan, S. Jiang, X. Han, Z. Chen, Formation of nanocrystalline AZ31B Mg alloys via cryogenic rotary swaging, J. Magnes. Alloy 11 (2023) 1580–1591.
[118] W.W. Jian, G.M. Cheng, W.Z. Xu, H. Yuan, M.H. Tsai, Q.D. Wang, C.C. Koch, Y. T. Zhu, S.N. Mathaudhu, Ultrastrong Mg alloy via nano-spaced stacking faults, Mater. Res. Lett. 1 (2013) 61–66.
[119] Q. Peng, Y. Sun, B. Ge, H. Fu, Q. Zu, X. Tang, J. Huang, Interactive contraction nanotwins-stacking faults strengthening mechanism of Mg alloys, Acta Mater. 169 (2019) 36–44.
[120] D.F. Shi, M.T. Pérez-Prado, C.M. Cepeda-Jiménez, Effect of solutes on strength and ductility of Mg alloys, Acta Mater. 180 (2019) 218–230.
[121] D. Zhang, K. Guan, Q. Yang, B. Jiang, C. Sun, N. Wang, B. Li, D. Zhang, X. Li, X. Liu, Z. Cao, J. Meng, Microstructures, mechanical properties and creep behavior of a Mg-3Yb-0.6Zn-0.4Zr casting alloy, Mater. Sci. Eng. A 745 (2019) 360–368.
[122] J. Lin, P. Fu, Y. Wang, H. Liu, Y. Zheng, L. Peng, W. Ding, Effect of La addition on microstructure, mechanical behavior, strengthening and toughening mechanisms of cast Mg-Gd-Zn alloy, Mater. Sci. Eng. A 866 (2023) 144688.
[123] Y. Zhang, Y. Wu, L. Peng, P. Fu, F. Huang, W. Ding, Microstructure evolution and mechanical properties of an ultra-high strength casting Mg-15.6Gd-1.8Ag-0.4Zr alloy, J. Alloy. Compd. 615 (2014) 703–711.
[124] J.A. Yasi, L.G. Hector Jr., D.R. Trinkle, First-principles data for solid-solution strengthening of magnesium: from geometry and chemistry to properties, Acta Mater. 58 (2010) 5704–5713.
[125] L. Gao, R.S. Chen, E.H. Han, Effects of rare-earth elements Gd and Y on the solid solution strengthening of Mg alloys, J. Alloy. Compd. 481 (2009) 379–384.
[126] A. Kula, X. Jia, R.K. Mishra, M. Niewczas, Flow stress and work hardening of Mg-Y alloys, Int. J. Plast. 92 (2017) 96–121.
[127] S.H. Kim, J.G. Jung, B.S. You, S.H. Park, Microstructure and texture variation with Gd addition in extruded magnesium, J. Alloy. Compd. 695 (2017) 344–350.
[128] N. Mo, I. McCarroll, Q. Tan, A. Ceguerra, Y. Liu, J. Cairney, H. Dieringa, Y. Huang, B. Jiang, F. Pan, M. Bermingham, M.X. Zhang, Understanding solid solution strengthening at elevated temperatures in a creep-resistant Mg-Gd-Ca alloy, Acta Mater. 181 (2019) 185–199.
[129] M. Xu, N. Li, X. Sha, Y. Liu, B. Gao, L. Xiao, X. Chen, H. Zhou, In-situ TEM observations on interaction of basal <a> dislocations and β' phases in a Mg-Gd binary alloy, Mater. Sci. Eng. A 841 (2022) 143017.
[130] T. Gladman, Precipitation hardening in metals, Mater. Sci. Technol. 15 (2013) 30–36.
[131] J. Jiang, S. Ni, H. Yan, N. Yan, M. Song, <c + a> dislocations shearing (0001)α plate precipitates in an Mg-Zn-Mn alloy, Scr. Mater. 170 (2019) 24–28.
[132] G.H. Park, J.T. Kim, H.J. Park, Y.S. Kim, H.J. Jeong, N. Lee, Y. Seo, J.Y. Suh, H. T. Son, W.M. Wang, J.M. Park, K.B. Kim, Development of lightweight Mg-Li-Al alloys with high specific strength, J. Alloy. Compd. 680 (2016) 116–120.
[133] H. Ji, G. Wu, W. Liu, X. Zhang, L. Zhang, M. Wang, Origin of the age-hardening and age-softening response in Mg-Li-Zn based alloys, Acta Mater. 226 (2022) 117673.
[134] F. Liu, R. Xin, C. Wang, B. Song, Q. Liu, Regulating precipitate orientation in Mg-Al alloys by coupling twinning, aging and detwinning processes, Scr. Mater. 158 (2019) 131–135.
[135] S. Celotto, TEM study of continuous precipitation in Mg-9 wt%Al-1 wt%Zn alloy, Acta Mater. 48 (2000) 1775–1787.
[136] W.J. Lai, Y.Y. Li, Y.F. Hsu, S. Trong, W.H. Wang, Aging behaviour and precipitate morphologies in Mg-7.7Al-0.5Zn-0.3Mn (wt%) alloy, J. Alloy. Compd. 476 (2009) 118–124.
[137] X.L. Ma, S.E. Prameela, P. Yi, M. Fernandez, N.M. Krywopusk, L.J. Kecskes, T. Sano, M.L. Falk, T.P. Weihs, Dynamic precipitation and recrystallization in Mg-9wt%Al during equal-channel angular extrusion: a comparative study to conventional aging, Acta Mater. 172 (2019) 185–199.
[138] N. Li, C. Wang, M.A. Monclús, L. Yang, J.M. Molina-Aldareguia, Solid solution and precipitation strengthening effects in basal slip, extension twinning and pyramidal slip in Mg-Zn alloys, Acta Mater. 221 (2021) 117374.
[139] X. Zhou, H. Yan, J. Chen, W. Xia, B. Su, L. Yu, W. Huang, M. Song, Effects of low temperature aging precipitates on damping and mechanical properties of ZK60 magnesium alloy, J. Alloy. Compd. 819 (2020) 152961.
[140] P. Peng, X. He, J. She, A. Tang, M. Rashad, S. Zhou, G. Zhang, X. Mi, F. Pan, Novel low-cost magnesium alloys with high yield strength and plasticity, Mater. Sci. Eng. A 766 (2019) 138332.
[141] Z. Yu, Y. Huang, L. Liu, K. Shi, B. Du, K. Liu, S. Li, W. Du, New strategy to solve the ambient strength-ductility dilemma in precipitation-strengthened Mg-Gd alloys via Li addition, Scr. Mater. 220 (2022) 114901.
[142] D. Lin, L. Wang, F. Meng, J. Cui, Q. Le, Effects of second phases on fracture behavior of Mg-10Gd-3Y-0.6Zr alloy, T. Nonferr. Met. Soc. 20 (2010) 421–425.
[143] I.A. Anyanwu, S. Kamado, Y. Kojima, Aging characteristics and high temperature tensile properties of Mg-Gd-Y-Zr alloys, Mater. Trans. 42 (2001) 1206–1211.
[144] X. Gao, J.F. Nie, Enhanced precipitation-hardening in Mg-Gd alloys containing Ag and Zn, Scr. Mater. 58 (2008) 619–622.
[145] T. Homma, N. Kunito, S. Kamado, Fabrication of extraordinary high-strength magnesium alloy by hot extrusion, Scr. Mater. 61 (2009) 644–647.
[146] Q. Wang, J. Chen, Z. Zhao, S. He, Microstructure and super high strength of cast Mg-8.5Gd-2.3Y-1.8Ag-0.4Zr alloy, Mater. Sci. Eng. A 528 (2010) 323–328.
[147] H. Zhou, G.M. Cheng, X.L. Ma, W.Z. Xu, S.N. Mathaudhu, Q.D. Wang, Y.T. Zhu, Effect of Ag on interfacial segregation in Mg-Gd-Y-(Ag)-Zr alloy, Acta Mater. 95 (2015) 20–29.
[148] L. Tang, C. Liu, Z. Chen, D. Ji, H. Xiao, Microstructures and tensile properties of Mg-Gd-Y-Zr alloy during multidirectional forging at 773K, Mater. Des. 50 (2013) 587–596.
[149] J.H. He, L. Jin, F.H. Wang, S. Dong, J. Dong, Mechanical properties of Mg-8Gd-3Y-0.5Zr alloy with bimodal grain size distributions, J. Magnes. Alloy 5 (2017) 423–429.
[150] C. You, C. Liu, Y. Wan, B. Tang, B. Wang, Y. Gao, X. Han, Dislocations-induced precipitates and their effect on mechanical properties of Mg-Gd-Y-Zr alloy, J. Magnes. Alloy 7 (2019) 414–418.
[151] J.L. Li, D. Wu, R.S. Chen, E.H. Han, Anomalous effects of strain rate on the room-temperature ductility of a cast Mg-Gd-Y-Zr alloy, Acta Mater. 159 (2018) 31–45.
[152] W.T. Sun, X.G. Qiao, M.Y. Zheng, C. Xu, S. Kamado, X.J. Zhao, H.W. Chen, N. Gao, M.J. Starink, Altered ageing behaviour of a nanostructured Mg-8.2Gd-3.8Y-1.0Zn-0.4Zr alloy processed by high pressure torsion, Acta Mater. 151 (2018) 260–270.
[153] S.M. He, X.Q. Zeng, L.M. Peng, X. Gao, J.F. Nie, W.J. Ding, Microstructure and strengthening mechanism of high strength Mg-10Gd-2Y-0.5Zr alloy, J. Alloy. Compd. 427 (2007) 316–323.
[154] S.M. He, X.Q. Zeng, L.M. Peng, X. Gao, J.F. Nie, W.J. Ding, Precipitation in a Mg-10Gd-3Y-0.4Zr (wt%) alloy during isothermal ageing at 250°C, J. Alloy. Compd. 421 (2006) 309–313.
[155] J.F. Nie, Effects of precipitate shape and orientation on dispersion strengthening in magnesium alloys, Scr. Mater. 48 (8) (2003) 1009–1015.
[156] E. Abe, Y. Kawamura, K. Hayashi, A. Inoue, Long-period ordered structure in a high-strength nanocrystalline Mg-1 at% Zn-2 at% Y alloy studied by atomic-resolution Z-contrast STEM, Acta Mater. 50 (2002) 3845–3857.
[157] J.K. Kim, W.S. Ko, S. Sandlöbes, M. Heidelmann, B. Grabowski, D. Raabe, The role of metastable LPSO building block clusters in phase transformations of an Mg-Y-Zn alloy, Acta Mater. 112 (2016) 171–183.
[158] Y.M. Zhu, A.J. Morton, J.F. Nie, The 18R and 14H long-period stacking ordered structures in Mg-Y-Zn alloys, Acta Mater. 58 (2010) 2936–2947.
[159] D. Egusa, E. Abe, The structure of long period stacking/order Mg-Zn-RE phases with extended non-stoichiometry ranges, Acta Mater. 60 (2012) 166–178.
[160] Y. Guo, Q. Luo, B. Liu, Q. Li, Elastic properties of long-period stacking ordered phases in Mg-Zn-Y and Mg-Ni-Y alloys: a first-principles study, Scr. Mater. 178 (2020) 422–427.
[161] Y. Zhou, Q. Luo, B. Jiang, Q. Li, F. Pan, Strength-ductility synergy in $Mg_{98.3}Y_{1.3}Ni_{0.4}$ alloy processed by high temperature homogenization and rolling, Scr. Mater. 208 (2022) 114345.
[162] C. Liu, Y. Zhu, Q. Luo, B. Liu, Q. Gu, Q. Li, A 12R long-period stacking-ordered structure in a Mg-Ni-Y alloy, J. Mater. Sci. Technol. 34 (2018) 2235–2239.
[163] S.R. Agnew, Ö. Duygulu, Plastic anisotropy and the role of non-basal slip in magnesium alloy AZ31B, Int. J. Plast. 21 (2005) 1161–1193.
[164] B.Y. Liu, F. Liu, N. Yang, X.B. Zhai, L. Zhang, Y. Yang, B. Li, J. Li, E. Ma, J.F. Nie, Z.W. Shan, Large plasticity in magnesium mediated by pyramidal dislocations, Science 365 (2019) 73–75.
[165] Z. Wu, W.A. Curtin, Intrinsic structural transitions of the pyramidal I <c + a> dislocation in magnesium, Scr. Mater. 116 (2016) 104–107.
[166] K. Wei, R. Hu, D. Yin, L. Xiao, S. Pang, Y. Cao, H. Zhou, Y. Zhao, Y. Zhu, Grain size effect on tensile properties and slip systems of pure magnesium, Acta Mater. 206 (2021) 116604.
[167] F. Wang, S.R. Agnew, Dislocation transmutation by tension twinning in magnesium alloy AZ31, Int. J. Plast. 81 (2016) 63–86.
[168] F. Wang, K. Hazeli, K.D. Molodov, C.D. Barrett, T. Al-Samman, D.A. Molodov, A. Kontsos, K.T. Ramesh, H. El Kadiri, S.R. Agnew, Characteristic dislocation substructure in $\{10\bar{1}2\}$ twins in hexagonal metals, Scr. Mater. 143 (2018) 81–85.
[169] A. Vinogradov, E. Vasilev, M. Linderov, D. Merson, In situ observations of the kinetics of twinning-detwinning and dislocation slip in magnesium, Mater. Sci. Eng. A 676 (2016) 351–360.
[170] J. Tu, S. Zhang, On the $\{10\bar{1}2\}$ twinning growth mechanism in hexagonal close-packed metals, Mater. Des. 96 (2016) 143–149.
[171] I. Basu, T. Al-Samman, Twin recrystallization mechanisms in magnesium-rare earth alloys, Acta Mater. 96 (2015) 111–132.

[172] X.L. Wu, K.M. Youssef, C.C. Koch, S.N. Mathaudhu, L.J. Kecskés, Y.T. Zhu, Deformation twinning in a nanocrystalline hcp Mg alloy, Scr. Mater. 64 (2011) 213–216.
[173] H. Xie, H. Pan, J. Bai, D. Xie, P. Yang, S. Li, J. Jin, Q. Huang, Y. Ren, G. Qin, Twin boundary superstructures assembled by periodic segregation of solute atoms, Nano Lett. 21 (2021) 9642–9650.
[174] K. Louca, H. Abdolvand, C. Mareau, M. Majkut, J. Wright, Formation and annihilation of stressed deformation twins in magnesium, Commun. Mater. 2 (2021) 9.
[175] T.W. Fan, B.Y. Tang, L.M. Peng, W.J. Ding, First-principles study of long-period stacking ordered-like multi-stacking fault structures in pure magnesium, Scr. Mater. 64 (2011) 942–945.
[176] K. Wei, L. Xiao, B. Gao, L. Li, Y. Liu, Z. Ding, W. Liu, H. Zhou, Y. Zhao, Enhancing the strain hardening and ductility of Mg-Y alloy by introducing stacking faults, J. Magnes. Alloy 8 (2020) 1221–1227.
[177] Z.R. Liu, D.Y. Li, The electronic origin of strengthening and ductilizing magnesium by solid solutes, Acta Mater. 89 (2015) 225–233.
[178] S. Sandlöbes, S. Zaefferer, I. Schestakow, S. Yi, R. Gonzalez-Martinez, On the role of non-basal deformation mechanisms for the ductility of Mg and Mg-Y alloys, Acta Mater. 59 (2011) 429–439.
[179] J. Jain, P. Cizek, K. Hariharan, Transmission electron microscopy investigation on dislocation bands in pure Mg, Scr. Mater. 130 (2017) 133–137.
[180] Z. Ding, W. Liu, H. Sun, S. Li, D. Zhang, Y. Zhao, E.J. Lavernia, Y. Zhu, Origins and dissociation of pyramidal <c + a> dislocations in magnesium and its alloys, Acta Mater. 146 (2018) 265–272.
[181] N. Zhou, Z. Zhang, L. Jin, J. Dong, B. Chen, W. Ding, Ductility improvement by twinning and twin-slip interaction in a Mg-Y alloy, Mater. Des. 56 (2014) 966–974.
[182] N. Stanford, R.K.W. Marceau, M.R. Barnett, The effect of high yttrium solute concentration on the twinning behaviour of magnesium alloys, Acta Mater. 82 (2015) 447–456.
[183] G.H. Huang, D.D. Yin, J.W. Lu, H. Zhou, Y. Zeng, G.F. Quan, Q.D. Wang, Microstructure, texture and mechanical properties evolution of extruded fine-grained Mg-Y sheets during annealing, Mater. Sci. Eng. A 720 (2018) 24–35.
[184] J.W. Lu, D.D. Yin, G.H. Huang, G.F. Quan, Y. Zeng, H. Zhou, Q.D. Wang, Plastic anisotropy and deformation behavior of extruded Mg-Y sheets at elevated temperatures, Mater. Sci. Eng. A 700 (2017) 598–608.
[185] A. Singh, H. Somekawa, T. Mukai, Dislocation structures in a near-isotropic Mg-Y extruded alloy, Mater. Sci. Eng. A 698 (2017) 238–248.
[186] L. Wang, Z. Huang, H. Wang, A. Maldar, S. Yi, J.S. Park, P. Kenesei, E. Lilleodden, X. Zeng, Study of slip activity in a Mg-Y alloy by in situ high energy X-ray diffraction microscopy and elastic viscoplastic self-consistent modeling, Acta Mater. 155 (2018) 138–152.
[187] B. Yin, Z. Wu, W.A. Curtin, First-principles calculations of stacking fault energies in Mg-Y, Mg-Al and Mg-Zn alloys and implications for <c + a> activity, Acta Mater. 136 (2017) 249–261.
[188] Y.F. Wu, S. Li, Z.G. Ding, W. Liu, Y.H. Zhao, Y.T. Zhu, Effect of charge redistribution factor on stacking-fault energies of Mg-based binary alloys, Scr. Mater. 112 (2016) 101–105.
[189] L. Tang, W. Liu, Z. Ding, D. Zhang, Y. Zhao, E.J. Lavernia, Y. Zhu, Alloying Mg with Gd and Y: increasing both plasticity and strength, Comput. Mater. Sci. 115 (2016) 85–91.
[190] H.Q. Sun, Y.N. Shi, M.X. Zhang, K. Lu, Surface alloying of an Mg alloy subjected to surface mechanical attrition treatment, Surf. Coat. Technol. 202 (2008) 3947–3953.
[191] J. Li, W. Xu, X. Wu, H. Ding, K. Xia, Effects of grain size on compressive behaviour in ultrafine grained pure Mg processed by equal channel angular pressing at room temperature, Mater. Sci. Eng. A 528 (2011) 5993–5998.
[192] R.B. Figueiredo, S. Sabbaghianrad, A. Giwa, J.R. Greer, T.G. Langdon, Evidence for exceptional low temperature ductility in polycrystalline magnesium processed by severe plastic deformation, Acta Mater. 122 (2017) 322–331.
[193] Z. Zeng, M. Zhou, P. Lynch, F. Mompiou, Q. Gu, M. Esmaily, Y. Yan, Y. Qiu, S. Xu, H. Fujii, C. Davies, J.F. Nie, N. Birbilis, Deformation modes during room temperature tension of fine-grained pure magnesium, Acta Mater. 206 (2021) 116648.
[194] Z. Zeng, J.F. Nie, S.W. Xu, C.H.J. Davies, N. Birbilis, Super-formable pure magnesium at room temperature, Nat. Commun. 8 (2017) 972.
[195] S.H.M. Azghandi, M. Weiss, B.D. Arhatari, J. Adrien, E. Maire, M.R. Barnett, A rationale for the influence of grain size on failure of magnesium alloy AZ31: an in situ X-ray microtomography study, Acta Mater. 200 (2020) 619–631.
[196] M.H. Yoo, Slip, twinning, and fracture in hexagonal close-packed metals, Metall. Mater. Trans. A 12 (1981) 409–418.
[197] K. Máthis, K. Nyilas, A. Axt, I. Dragomir-Cernatescu, T. Ungár, P. Lukáč, The evolution of non-basal dislocations as a function of deformation temperature in pure magnesium determined by X-ray diffraction, Acta Mater. 52 (2004) 2889–2894.
[198] A. Chapuis, J.H. Driver, Temperature dependency of slip and twinning in plane strain compressed magnesium single crystals, Acta Mater. 59 (2011) 1986–1994.
[199] G.D. Sim, K.Y. Xie, K.J. Hemker, J.A. El-Awady, Effect of temperature on the transition in deformation modes in Mg single crystals, Acta Mater. 178 (2019) 241–248.
[200] N.M. Ventura, P. Schweizer, A. Sharma, M. Jain, T.E.J. Edwards, J.J. Schwiedrzik, C. Peruzzi, R.E. Logé, J. Michler, X. Maeder, Micromechanical response of pure magnesium at different strain rate and temperature conditions: twin to slip and slip to twin transitions, Acta Mater. 243 (2023) 118528.
[201] W.F. Hosford, E.W. Kelley, Plane-strain compression of magnesium and magnesium alloy crystals, Trans. Metall. Soc. Aime. 242 (1968) 5–13.
[202] H.Y. Yoshinaga, R. Horiuchi, On the nonbasal slip in magnesium crystals, Trans. Jpn. Inst. Met. 5 (1964) 14–21.
[203] B.C. Wonsiewicz, W.A. Backofen, Plasticity of magnesium single crystals, Trans. Met. Soc. AIME 239 (1967) 1422–1431.
[204] T. Obara, H. Yoshinga, S. Morozumi, $\{11\bar{2}2\} < \bar{1}\bar{1}23 >$ Slip system in magnesium, Acta Met. 21 (1973) 845–853.
[205] Z.Y. Meng, C. Wang, Z.M. Hua, M. Zha, H.Y. Wang, Achieving extraordinary thermal stability of fine-grained structure in a dilute magnesium alloy, Mater. Res. Lett. 10 (2022) 797–804.
[206] Z. Zhang, J. Xie, J. Zhang, X.S. Yang, R. Wu, Towards designing high mechanical performance low-alloyed wrought magnesium alloys via grain boundary segregation strategy: a review, J. Magnes. Alloy 12 (2024) 1774–1791.
[207] X. Zhuo, L. Zhao, W. Gao, Y. Wu, H. Liu, P. Zhang, Z. Hu, J. Jiang, A. Ma, Recent progress of Mg-Sn based alloys: the relationship between aging response and mechanical performance, J. Mater. Res. Technol. 21 (2022) 186–211.
[208] W. Sun, Y. Deng, Y. Hu, H. Zhan, K. Yan, S. Shuai, E. Guo, Z. Zheng, G. Zeng, Enhanced high-temperature strength of a Mg-4Sn-3Al-1Zn alloy with good thermal stability via Mg_2Sn precipitation, J. Magnes. Alloy (2025) (In Press).
[209] D. Xie, H. Pan, Z. Pan, T. Fu, Z. Zeng, H. Xie, Y. Ren, W. Tang, G. Qin, Achieving outstanding heat-resistant properties in Mg alloy via constructing stable solute-network, Mater. Res. Lett. 11 (2023) 374–382.
[210] K.A. Darling, B.K. VanLeeuwen, C.C. Koch, R.O. Scattergood, Thermal stability of nanocrystalline Fe-Zr alloys, Mater. Sci. Eng. A 527 (2010) 3572–3580.
[211] H. Fu, X. Qian, S. Xu, B. An, R. Pan, B. Jiang, Y. Zeng, Room- and elevated-temperature strength of as-cast Mg-Sn-Y alloys mediated by Sn and Y solubility via intrinsic stability and deformation resistance, J. Mater. Res. Technol. 33 (2024) 6633–6640.
[212] N. Liang, Y. Zhao, A review on thermal stability of nanostructured materials, J. Alloy. Compd. 938 (2023) 168528.
[213] C.C. Koch, R.O. Scattergood, K.A. Darling, J.E. Semones, Stabilization of nanocrystalline grain sizes by solute additions, J. Mater. Sci. 43 (2008) 7264–7272.
[214] M. Bugnet, A. Kula, M. Niewczas, G.A. Botton, Segregation and clustering of solutes at grain boundaries in Mg-rare earth solid solutions, Acta Mater. 79 (2014) 66–73.
[215] M. Kuzmina, M. Herbig, D. Ponge, S. Sandlöbes, D. Raabe, Linear complexions: Confined chemical and structural states at dislocations, Science 349 (2015) 1080–1083.
[216] J.F. Nie, Y.M. Zhu, J.Z. Liu, X.Y. Fang, Periodic segregation of solute atoms in fully coherent twin boundaries, Science 340 (2013) 957–960.
[217] L.R. Xiao, Y. Cao, S. Li, H. Zhou, X.L. Ma, L. Mao, X.C. Sha, Q.D. Wang, Y.T. Zhu, X.D. Han, The formation mechanism of a novel interfacial phase with high thermal stability in a Mg-Gd-Y-Ag-Zr alloy, Acta Mater. 162 (2019) 214–225.
[218] L.R. Xiao, X.F. Chen, Y. Cao, H. Zhou, X.L. Ma, D.D. Yin, B. Ye, X.D. Han, Y.T. Zhu, Solute segregation assisted nanocrystallization of a cold-rolled Mg-Ag alloy during annealing, Scr. Mater. 177 (2020) 69–73.
[219] X.F. Chen, L.R. Xiao, Z.G. Ding, W. Liu, Y.T. Zhu, X.L. Wu, Atomic segregation at twin boundaries in a Mg-Ag alloy, Scr. Mater. 178 (2020) 193–197.
[220] Q. Su, R. Wang, T. Li, Y. Han, L. Hu, J. Zhou, G. Zhao, X. Wang, H. Yu, Effect of Ti addition on the thermal stability of nanocrystalline AZ61 Mg alloy, J. Alloy. Compd. 905 (2022) 164266.
[221] Q. Su, R. Wang, H. Yu, H. Li, J. Zhou, D. Wang, L. Hu, The effect of submicron SiC particles on the thermal stability of nanocrystalline AZ9, 1 Alloy, J. Mater. Res. Technol. 22 (2023) 519–530.
[222] H. Zhang, J. Sun, K. Chen, H. Zhou, J. Jia, Z. Wang, Y. Lu, K. Gao, W. Ma, Microstructure and thermal stability of nanocrystalline AZ31 Mg alloys reinforced by ultrafine vanadium particles, J. Mater. Res. Technol. 23 (2023) 943–953.
[223] E. Gerashi, M. Asadollahi, R. Alizadeh, R. Mahmudi, Effects of Sr additions on the microstructural stability and mechanical properties of a cast Mg-4Zn alloy, Mater. Sci. Eng. A 843 (2022) 143127.
[224] Z. Xiao, S. Xu, W. Huang, C. Jin, Z. Lin, Stability and elastic anisotropy of the β′ and γ′′ phases in Mg-Gd-Ag alloys at finite temperatures by first principles calculations, J. Mater. Res. Technol. 33 (2024) 9195–9207.